L.A. Kisling ED22

LMSC-HEC TR F268584-I

FINAL REPORT

SPACE SHUTTLE MAIN ENGINE STRUCTURAL ANALYSIS AND DATA REDUCTION/EVALUATION

VOLUME 1: AFT SKIRT ANALYSIS

April 1989

Contract NAS8-37282

Prepared for

NATIONAL AERONAUTICS AND SPACE ADMINISTRATION
GEORGE C. MARSHALL SPACE FLIGHT CENTER, AL 35812

by

David M. Berry

Lockheed
Missiles & Space Company, Inc.
Huntsville Engineering Center
4800 Bradford Blvd., Huntsville, AL 35807

FOREWORD

This volume of the final report summarizes the analysis performed on the Space Shuttle Solid Rocket Booster Aft Skirt under Contract NAS8-37282. Using the ANSYS finite element program, a global model of the Aft Skirt and a detailed nonlinear model of the failure region were made. The analysis was performed by David Berry and Mark Stansberry.

CONTENTS

CONTENTS (Continued)

LIST OF TABLES

LIST OF FIGURES

1. INTRODUCTION

1.1 PROBLEM DEFINITION

During the STA-2B test of the Space Shuttle Solid Rocket Booster (SRB) Aft Skirt and motorcase, the Aft Skirt was damaged in the form of a crack along the post to skin weld on the right hand side of holddown post 8. The crack formed at approximately 129% of STA-2B limit load. Previous analyses had shown a positive margin based on ultimate strength at 140% of limit load, and the Aft Skirt had passed an earlier test using an older set of load data (STA-1).

A post-test assessment resulted in the following determinations:

(1) The STA -2B loads caused a more severe local bending at the post to skin weld and the current finite element models, which were developed for the STA-1 loads, were too coarse and could not accurately predict the stress at this location. Therefore a new, more detailed, independent analysis was required. It was also determined that, for complete independence, this analysis should use a different finite element program than the one currently used in the analysis of the Aft Skirt.

(2) A very detailed nonlinear plastic model of the failure area was needed to explain the failure mechanism.

During the course of the analysis task, the bracketry in and around the aft ring of the Aft Skirt was redesigned in an attempt to strengthen the Aft Skirt and eliminate the failure mode seen in the STA-2B test. Therefore the scope of the analysis was enlarged to include the redesigned structure.

The redesigned Aft Skirt was then tested under a new set of loads known as the STA-3 loads. A crack formed in the same location during this test at approximately 132% of the STA-3 limit loads. The pretest analysis had predicted that the strain levels in the critical area of the post forging-to-weld interface would be 40% less than those seen during the STA-2B test. The pretest analysis was then studied, using typical material properties and material properties from tests of Aft Skirt specimens instead of from handbooks.

1.2. SUMMARY

The analysis has confirmed the area of failure in both STA-2B and STA-3 tests as the forging heat affected zone (HAZ) at the aft ring centerline. The highest hoop strain in the HAZ occurs in this area. However, the analysis *does not* predict failure as defined by ultimate elongation of the material equal to 3.5% total strain.

The analysis correlates well with strain gage data from both the Wyle influence test of the original design Aft Skirt and the STA-3 test of the redesigned Aft Skirt.

We suggest that the sensitivity of the failure area material strength and stress/strain state to material properties and therefore to small manufacturing or processing variables is the most likely cause of failure below the expected material ultimate properties.

2. APPROACH

Lockheed Huntsville Engineering Center (HEC) personnel decided that a completely new finite element model of the Aft Skirt was needed. This would insure complete independence and would be more detailed throughout than the existing models. This new global model could then be used, if needed, to analyze any or every component of the Aft Skirt. It was decided that the global model would consist of a 180° section of the Aft Skirt, thus using the geometric symmetry of the Aft Skirt to reduce the model size. To model the unsymmetrical STA-2B loading accurately, both symmetric and antisymmetric boundary conditions would be used and the loads broken into symmetric and antisymmetric components. These would then be combined to give the solution for the unsymmetrical loading.

Paralleling this effort would be the construction of a detailed nonlinear model of the failure region. This model could be more detailed than would be possible in the global model of the entire Aft Skirt.

It was decided to use the ANSYS finite element program, a well known program available on the Marshall Space Flight Center (MSFC) Cray and IBM computers. These computers would be needed to execute the very large model needed to give sufficiently accurate results. ANSYS also has a large element library with nonlinear, plastic, substructuring, and submodeling capability, all of which would be needed in this analysis.

3. ANALYSIS OF THE ORIGINAL DESIGN (STA-2B FAILURE)

3.1 GLOBAL MODEL

3.1.1 Modeling Procedure

Personnel from other Lockheed organizations were brought in to help develop the global model of the Aft Skirt. These were Patrick Batdorf (GELAC), Kirby Pool (MSD), and Kenneth Sakai (MSD).

The finite element model was built with more detail than the existing models. In order to execute, even on the Cray X-MP, the model was separated into substructures. The modeling tasks were divided by geometrically similar sections of the Aft Skirt. One person modeled the holddown posts, another modeled the ring segments, and another modeled the skin segments. Communication was maintained to assure model continuity at the interfaces between sections modeled by different people. This practice was found to be especially important.

ANSYS was not available on any Lockheed computer at the start of this program and Kirby Pool and Kenneth Sakai were not familiar with ANSYS but were very familiar with the Lockheed DIAL finite element program which was available on both the HEC and MSD VAXs as well as the Lockheed Cray. Therefore, after comparing the ANSYS and DIAL input formats, it was decided to build the models using the program most familiar to the analysts (in this case DIAL) and convert to ANSYS to perform the analysis. Using this approach, Kirby Pool modeled the holddown posts and Kenneth Sakai modeled the skin and skin stiffeners using DIAL.

Patrick Batdorf modeled the ring sections and gussets using the CADAM system mesh processor. The CADAM scopes were located in the Lockheed HEC but were connected to IBM mainframes located at the GELAC facility in Georgia. The CADAM mesh software created NASTRAN input data files which were then transferred by ASCII tape to the Lockheed VAX network. While on the VAX network, the files were transferred electronically to a MSD VAX in Sunnyvale CA. Here they were converted into DIAL input data using a FORTRAN program written by Kenneth Sakai.

The component models were checked individually and were then assembled into one large DIAL data base. DIAL was then used on the Lockheed Cray to merge coincident nodes, find nodes that should be coincident but were not, and renumber nodes and elements. When this process was completed and known errors were corrected, the DIAL data base contained the entire global model with each node numbered consecutively. Each substructure was then extracted in ANSYS format from this data base by selecting nodes and elements based on geometric regions.

3.1.2 Size and Description of the Model

The ANSYS global finite element model of the SRB Aft Skirt is a model of a symmetric 180° section of the Aft Skirt. The model contains two holddown posts 60° apart. The model boundaries are the tiedown points on the holddown post shoes, the symmetry plane at $\theta = 0$ and $\theta = 180°$, and the motorcase at approximately 100 in. above the top ring.

This model contains 85,459 nodes connected by 40,617 solid elements and 12,518 shell elements. The total number of degrees of freedom (DOF) in the global model of the Aft Skirt is 293,914. Due to the large size of this model, it is divided into 20 substructures. The geometric layout of the substructures is shown in Figure 1. Plots of the individual substructures are shown in Appendix A.

3.1.3 Execution Procedure

The substructuring procedure used in ANSYS required that this analysis be broken into four parts: substructure generation, use pass, unit load stress pass, and load combination.

Substructure generation is done for each substructure individually. This takes the basic input data (nodal coordinates, element connectivity, etc.) and creates three files: FILE2, FILE3 and FILE8. FILE2 and FILE3 contain element and geometry data that are not used until the stress recovery pass is made for that substructure. FILE8 contains the information necessary to define that substructure in the use pass. The total CPU time required for the generation of all 20 substructures was over 4 CPU hours on the MSFS EADS Cray. Table 1 contains a summary of the total DOF, boundary DOF, maximum wavefront, and generation time for the substructures.

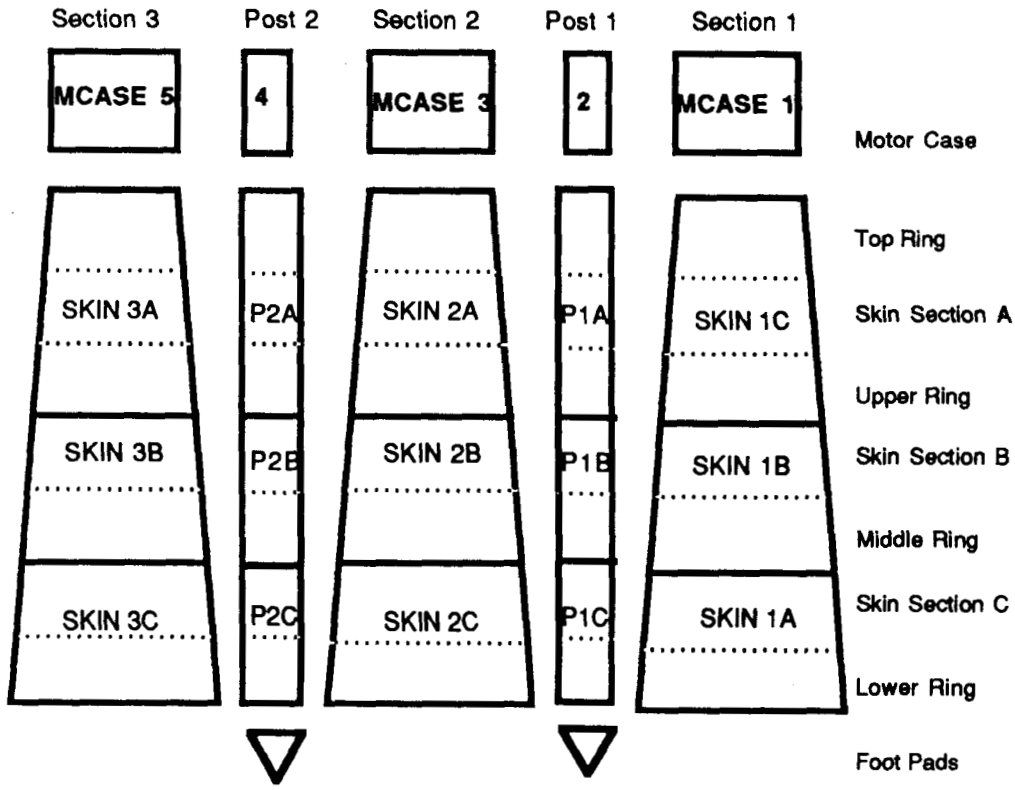

Figure 1. Aft Skirt Substructure Boundaries

Table 1. AFT SKIRT SUBSTRUCTURE STATISTICS

SUBSTRUCTURE	DEGREES OF FREEDOM	BOUNDARY DEGREES OF FREEDOM	MAXIMUM WAVEFRONT	GENERATION RUN TIME (cpu sec)
1 MCASE 1	4784	315	454	55
2 SKIN 1A	22481	1103	1414	1371
3 SKIN 1B	20293	1092	1476	1031
4 SKIN 1C	22014	840	1311	1114
5 MCASE 2	1913	279	396	30
6 POST 1A	9120	1147	1391	455
7 POST 1B	12411	1305	1683	654
8 POST 1C	21671	1053	1542	1299
9 MCASE 3	3819	369	486	46
10 SKIN 2A	18271	1007	1331	1021
11 SKIN 2B	17262	960	1321	798
12 SKIN 2C	18292	774	1255	845
13 MCASE 4	1913	279	1408	31
14 POST 2A	8931	1182	1249	451
15 POST 2B	12402	1314	1638	622
16 POST 2C	21668	1053	1542	1239
17 MCASE 5	4778	414	528	55
18 SKIN 3A	21265	1071	1406	1321
19 SKIN 3B	19933	1092	1522	1009
20 SKIN 3C	21855	840	1331	1103

The Use pass is an execution which solves for displacements of the boundary DOFs of the substructures. It uses the FILE8s created by the generation runs of all the individual substructures and creates a FILE13 which contains the displacements of the boundary nodes of the substructures. The use pass contained 6374 active DOFs and required 3.5 million words of memory and more than one CPU hour of processing time on the MSFC Cray XMP.

The unit load stress pass for each substructure uses the FILE2 and FILE3 created by the substructure generation pass and the FILE13 created by the use pass. This gives a solution for 12 load cases made up of unit loads applied in each direction on each holddown post footpad for both symmetry and antisymmetry boundary conditions.

The load combination pass takes each of the unit load cases, multiplies it by the appropriate factor, and adds the load cases together to obtain the solution for a real unsymmetrical loading condition.

3.2. DETAILED MODEL

3.2.1. Modeling Procedure

David Berry of Lockheed HEC was responsible for developing the nonlinear detailed model of the Aft Skirt failure area. The detailed model was created using the DIAL program and then converted to ANSYS input data on the HEC VAX. These input data were transferred to the MSFC IBM by ASCII tape.

3.2.2. Size and Description of Model

The detailed model describes the portion of the Aft Skirt from the bottom of the skirt to an upward point 13 in. above the bottom of the post and from the inside edge of the post leg to approximately 3 in. on the skin side of the weld. The detailed model included the Aft Ring and associated bracketry when the USBI NASTRAN model was used for boundary conditions. This detailed model configuration is shown in Figure 2. However, the ANSYS global model developed by Lockheed contained enough detail to move the boundary of the detailed model to the horizontal and vertical tabs as shown in Figures 3 and 4. This eliminated a considerable number of nodes and elements from the nonlinear solution.

In its final form the detailed model contained approximately 3000 nodes. It was made completely of eight node brick elements (denoted as STIF45 in ANSYS).

3.2.3. Execution Procedure

3.2.3.1. USBI Global Boundaries

The detailed model was completed before the global model of the Aft Skirt. In the interest of quick preliminary results, boundary conditions for this model were first obtained from the existing NASTRAN model of the Aft Skirt. This model was created and being used by USBI. Personnel from USBI allowed Lockheed personnel to copy this model; they also explained the execution procedure. This model was then executed by Lockheed for the proper load case.

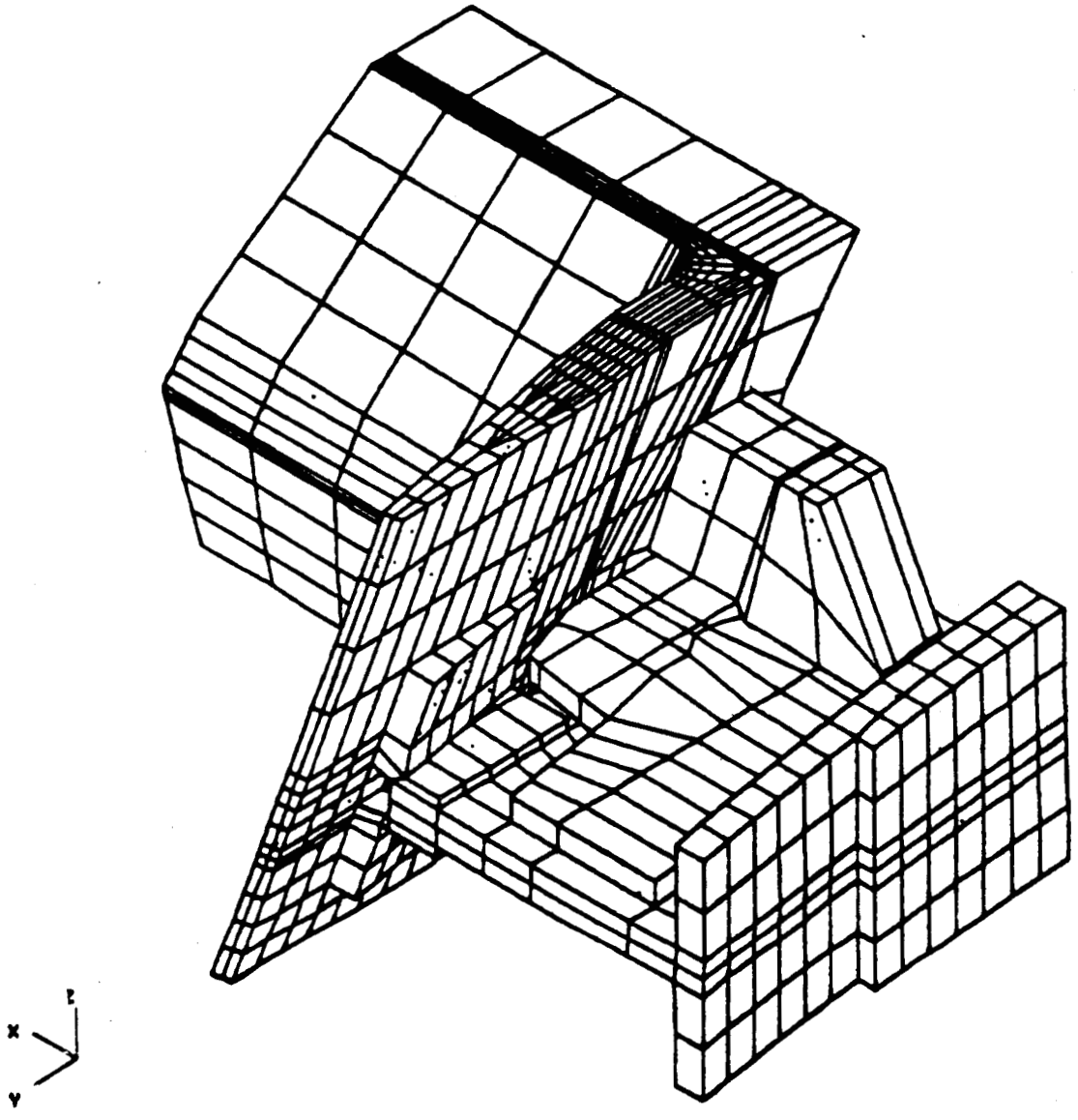

Figure 2. Aft Skirt Detailed Model Used with NASTRAN Global Model

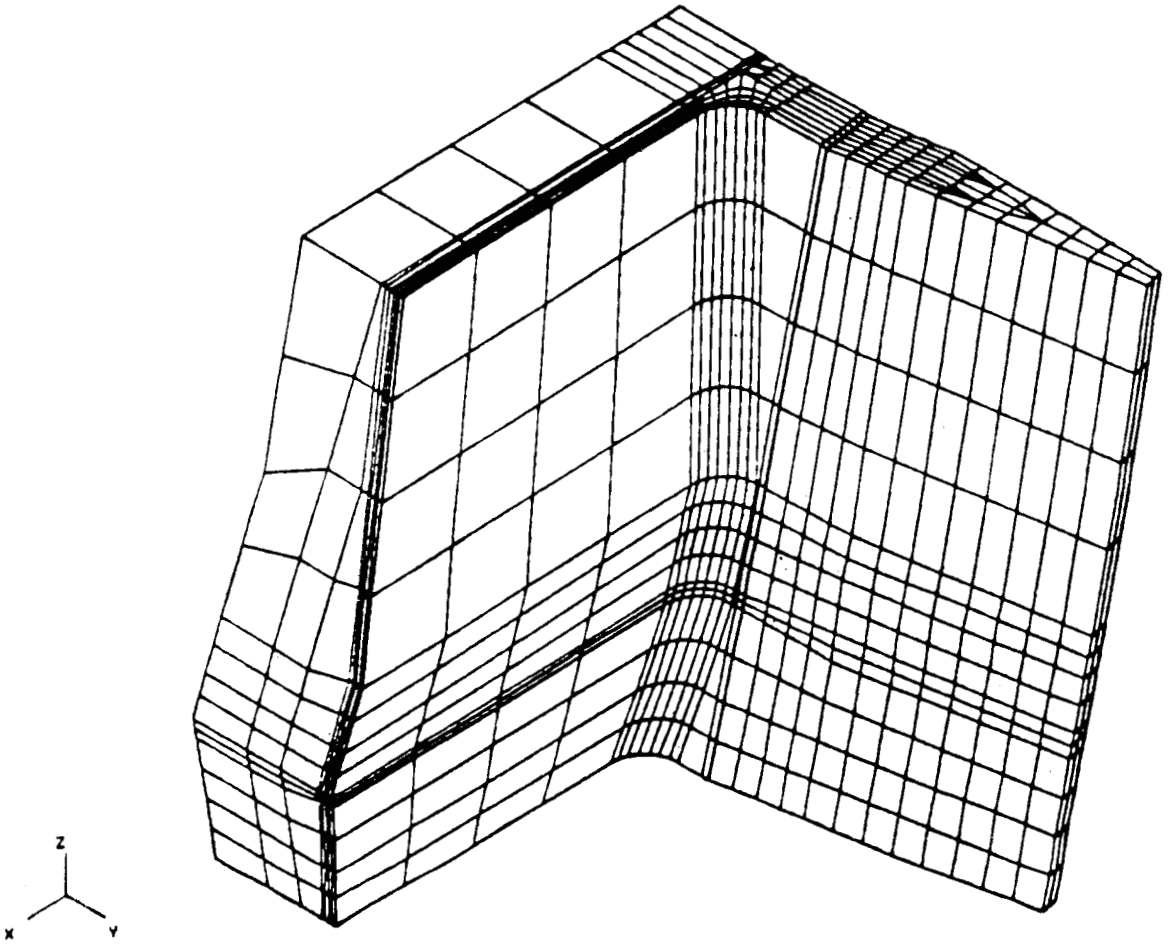

Figure 3 Aft Skirt Detailed Model (Front View)

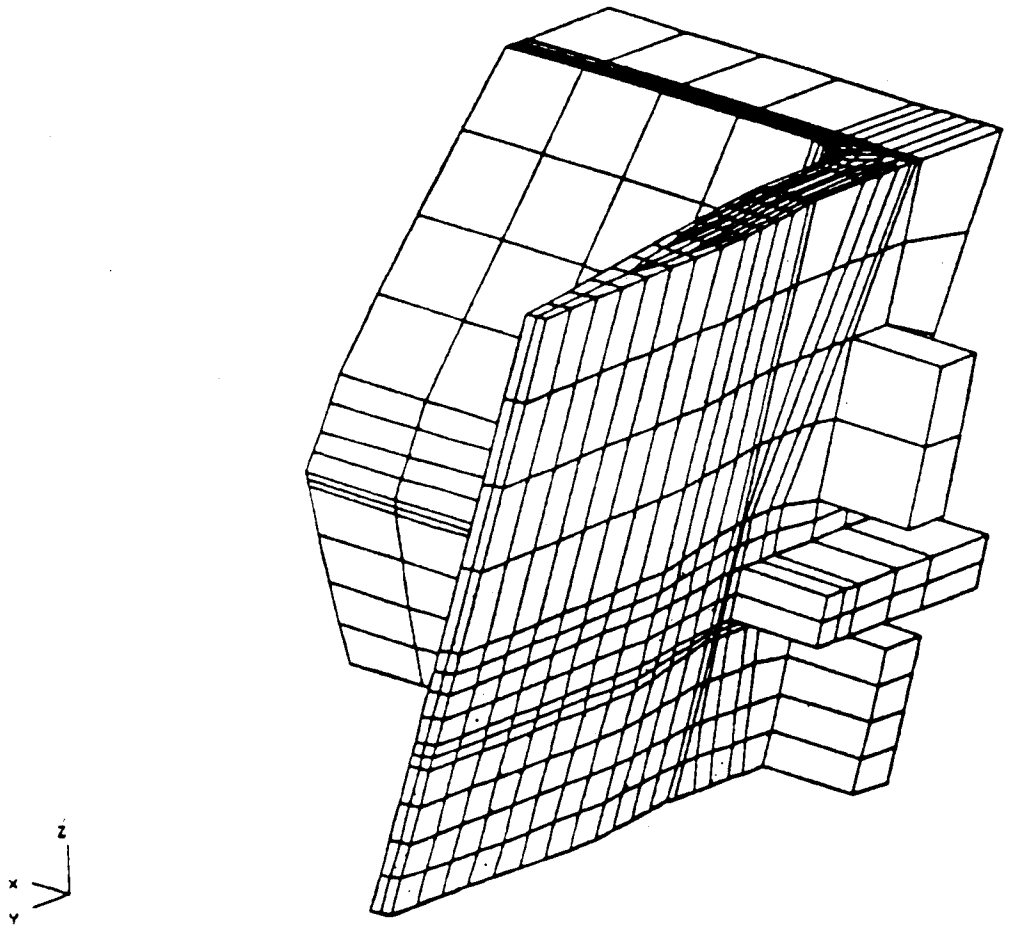

Figure 4. Aft Skirt Detailed Model (View from Inside Skirt)

In order to transfer the results from this model to the ANSYS detailed model, the ANSYS submodeling procedure was used. (This procedure allows a portion of a finite element model to be modeled in finer detail without the analyst being required to make the transition from a coarse to a finer mesh. The finer model is a separate model representing the area where more detail is needed. Displacements are interpolated from the coarse model to the boundaries of the finer model using the element shape functions.) In this case a "boundary model" was created in ANSYS which exactly duplicated the nodal coordinates and element connectivity of the portion of the NASTRAN model which included the geometric boundaries of the ANSYS detailed model. The displacements from the NASTRAN model were applied to this "boundary model." It was then possible to use the ANSYS submodeling procedure to interpolate these displacements and apply them to the detailed ANSYS model of the Aft Skirt.

The displacements determined by the submodel interpolation were used as boundary conditions for a linear solution using the detailed model. Boundary forces obtained from this linear solution were used as applied loads for nonlinear analysis of the Aft Skirt failure region.

3.2.3.2. Lockheed Global Boundaries

After the Lockheed global model of the Aft Skirt had been completed, checked out, and executed on the MSFC Cray, it could then be used to supply boundary conditions for the detailed model of the failure area. The substructure referred to in Table 1 as post 2C (equivalent to the lower portion of holddown post 8) was used to obtain these boundary conditions. Using the submodel procedure, displacements to be applied to the boundaries of the detailed model were interpolated directly from the FILE12 created during the stress pass of post 2C.

The displacements determined by the submodel interpolation were used as boundary conditions for a linear solution using the detailed model. Boundary forces obtained from this linear solution were used as applied loads for nonlinear analysis of the Aft Skirt failure region.

3.3. RESULTS

Results were first obtained for the following three loading conditions:
STA-1: Loads applied during the test which the Aft Skirt passed
STA-2B: Loads that caused structural damage to the Aft Skirt during a test
IVBC-3: Most recent design loads.

3.3.1. Global Model

At this time the global model was used primarily to obtain boundary conditions for the detailed model, but it was also used to examine stress distribution over a larger area of the structure. The largest maximum principal stress in the post 2C substructure occurred in the post fillet area near the aft ring centerline for each load case. The largest maximum principal stress for STA-1 loads is 46 ksi. For STA-2B loads the stress increases 33% to 61 ksi. The IVBC-3 loads cause an additional 6% increase in stress to 64 ksi.

The linear global model does not agree well with the STA-2B strain gage data in the high strain areas at 129% of limit load. This is as expected and is due to the effects of plastic behavior of the material in this region and the global model lacking sufficient detail to account for the stress concentrations and high stress gradients encountered in the lower portion of the skirt near the failure region.

When the model is compared with gages located away from these effects the results improve. Gages S5171, S5172, S5184, and S5185, located on the front of the post legs approximately 15 and 20 in. from the bottom of the post, differ from the global model prediction by 19 to 25%.

Gages T5332 and T5411, located at the top of the post, differ from analysis by 14 and 15 %, respectively, in hoop strain and by 7 and 2%, respectively, in axial (z) strain.

3.3.2. Detailed Model Using NASTRAN Global Model Boundary

The results of the linear analyses are shown in Table 2. The increased stress is due to the more detailed model showing the stress concentration caused by the post fillet. The post fillet area is the highest stressed area, but the material in this area is stronger due to its

distance from the weld. The failure location in the STA-2B test was in the heat affected material on the post forging side of the weld. The linear analysis stresses in the heat affected material increase 24% to 61 ksi due to STA-2B loads.

Table 2. LINEAR MODEL USING NASTRAN GLOBAL MODEL BOUNDARY

Load Case	Post Fillet Area		Heat Affected Zone	
	Max. Principal Stress (ksi)	% Increase	Max. Principal Stress (ksi)	% Increase
STA-1	117.		49.	
STA-2B	140.	20%	61.	24%
IVBC-3	143.	22%	62.	27%

The nonlinear analysis results are shown in Table 3. The equivalent plastic strain in the post fillet reaches 4.2 % for the STA-2B load case as opposed to 1.9 % for the STA-1 load case. This is an increase of 121%. In the HAZ the equivalent plastic strain increases from 0.9% for the STA-1 loads to 2.1% for STA-2B loads. This is an increase of 133%.

Table 3. NONLINEAR MODEL USING NASTRAN GLOBAL MODEL BOUNDARY

Load Case	Highest Strained Area (bottom of post fillet)		Heat Affected Zone	
	Equivalent Plastic Strain(%)	% Increase	Equivalent Plastic Strain(%)	% Increase
STA-1	1.9		0.9	
STA-2B	4.2	121%	2.1	133%

Following are the results of the linear analyses using the NASTRAN global model for boundary conditions.

(1) All three load cases cause stresses exceeding material yield stress.
(2) STA-2B loads cause stresses 20% higher than STA-1 loads.
(3) IVBC-3 loads cause stresses slightly higher (3 to 6%) than STA-2B loads.
(4) The detailed model shows stress concentration effects which the global model is too coarse to show.

Following are the results of the nonlinear analyses using the NASTRAN global model for boundary conditions.

(1) STA-2B loads cause plastic strains two times higher than STA-1 loads.
(2) The highest plastic strains occur in the post fillet area.
(3) The strains are due primarily to local bending.

3.3.3. Detailed Model Using ANSYS Global Model Boundary

Using the LMSC global ANSYS model for boundary conditions, the maximum stresses predicted by a linear analysis using the detailed model occur in the forging material in the post fillet area. For STA-1 loads, the maximum principal stress in this region is 80 ksi. This increases 26% to 101 ksi for the STA-2B loads. The maximum principal stress in the HAZ increases from 46 ksi for the STA-1 loads to 63 ksi for the STA-2B loads, an increase of 37%.

Using the LMSC global ANSYS model for boundary conditions, the maximum equivalent plastic strain predicted by the nonlinear analysis occurs in the forging material in the fillet area. For the STA-1 loads, the maximum strain is 0.61%. This increases 179% to a value of 1.7% strain for the STA-2B loads. The maximum equivalent strain in the HAZ increases from 0.38% for STA-1 loads to 1.4% for STA-2B loads, for an increase of 268%. This is shown in Table 4.

Table 4. NONLINEAR MODEL USING ANSYS GLOBAL MODEL BOUNDARY

Load Case	Highest Strained Area		Heat Affected Zone	
	Equivalent Plastic Strain(%)	% Increase	Equivalent Plastic Strain(%)	% Increase
STA-1	0.61		0.38	
STA-2B	1.7	179%	1.4	268%

One of the most significant aspects of this analysis is plastic strain versus load. This is shown in Figure 5. The plastic strain in the HAZ due to STA-2B loads increases very rapidly, while that due to STA-1 loads increases more slowly. This phenomenon, peculiar to nonlinear analyses, indicates that a small increase in load will cause a nonproportionally large increase in strain. Such an increase leads to instability in the analytical model and indicates impending gross plastic yielding. Because of this, the judgment was that, although the finite element model does not predict failure by the absolute value of plastic strain, the strain-versus-load curve is in a region where a small inaccuracy could greatly increase the strain predicted.

The following is a summary of results of the nonlinear analyses using the ANSYS global model for boundary conditions.

(1) STA-2B loads cause strains almost three times higher than STA-1 loads.
(2) The highest plastic strains occur in the post fillet area.
(3) The strain state of the post fillet with respect to STA-2B loads is such that a small increase in load will cause a nonproportionally large increase in strain.

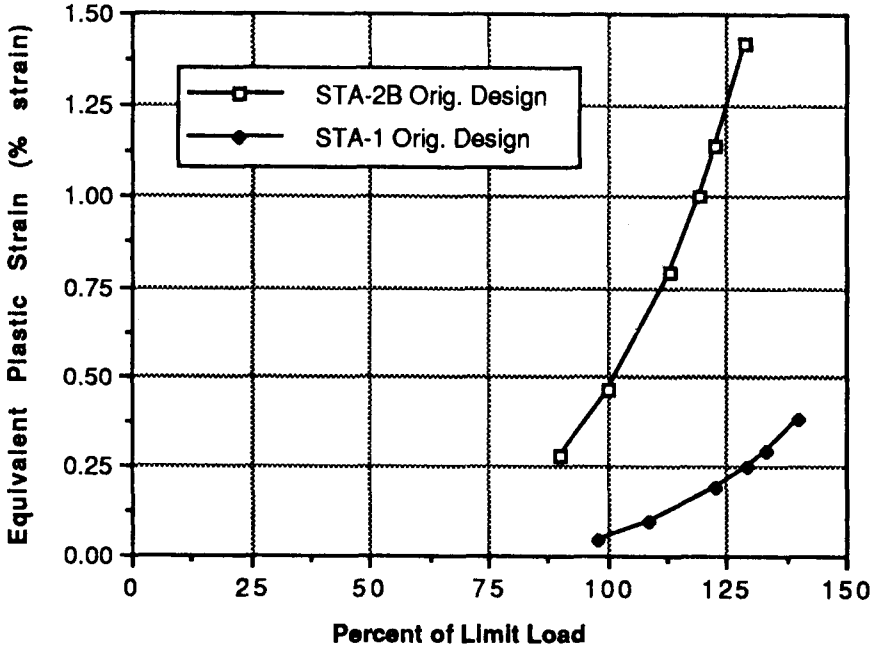

Figure 5. Plastic Strain in HAZ versus Percent Limit Load

The detailed model was correlated with strain gage data from the SRB Aft Skirt Influence Test Program (Wyle Laboratories Report No. 48915-02). Data from eight strain gages, located as shown in Figure 6, were compared for "unit" loads applied to post 8. The comparison for each load case is shown graphically in Figures 7 through 9 and numerically in Table 5. For the radial and axial loads the model differed from the strain gages by an average of 6.6% and a maximum of 12%. The tangential load caused a higher percentage of difference between the model and the gages, but this is believed to be due to the lower magnitude of the stresses caused by this load.

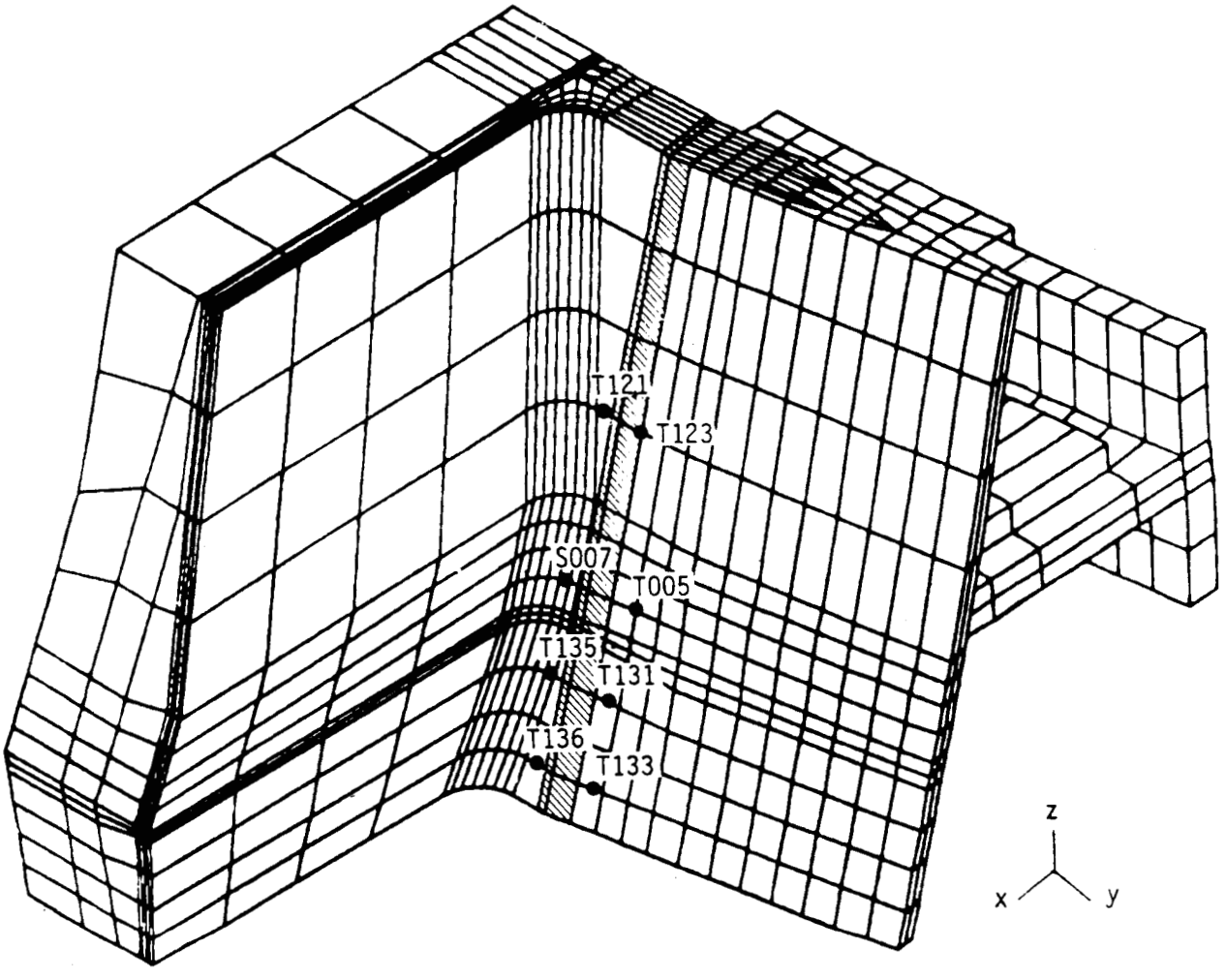

Figure 6. Wyle Influence Test Strain Gage Locations

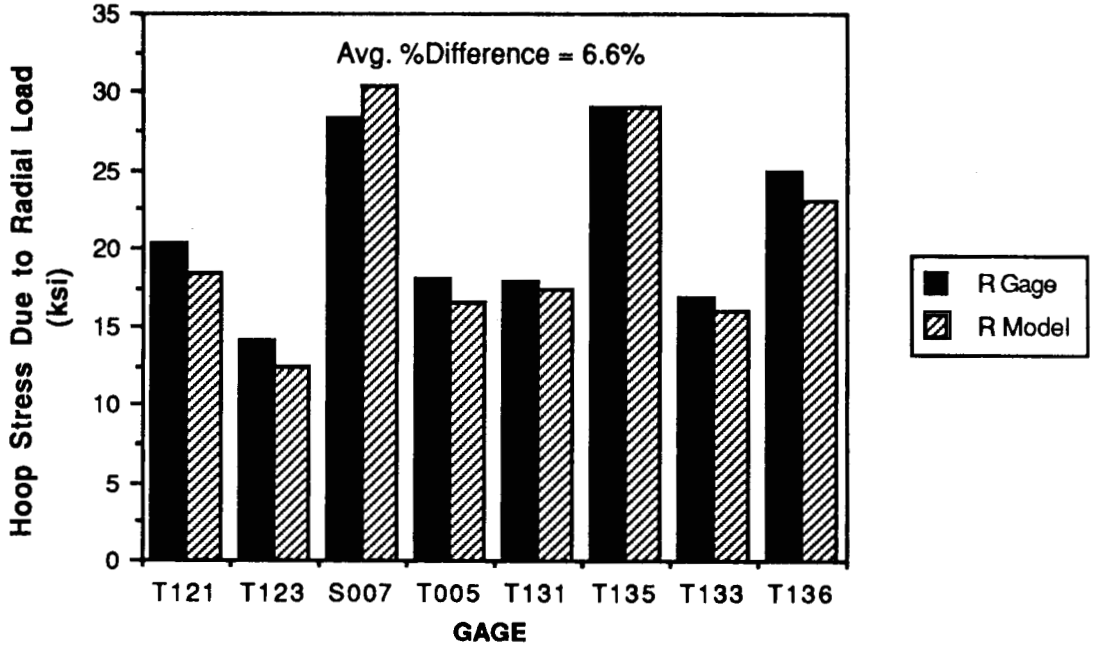

Figure 7. Strain Gage Correlation for Radial Applied Load

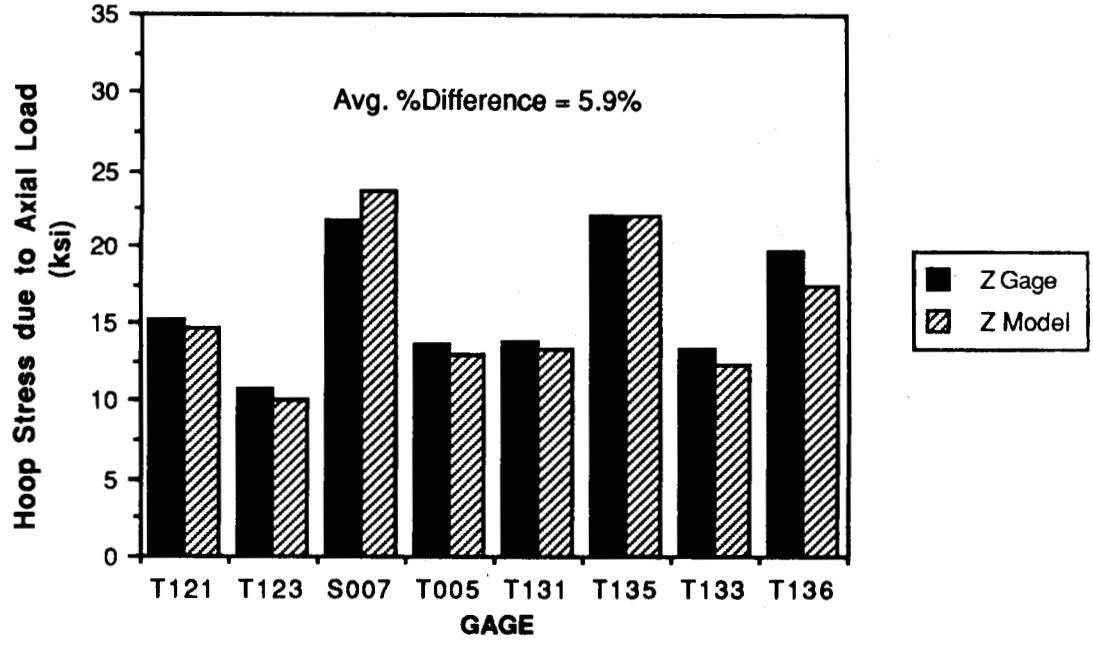

Figure 8. Strain Gage Correlation for Axial Applied Load

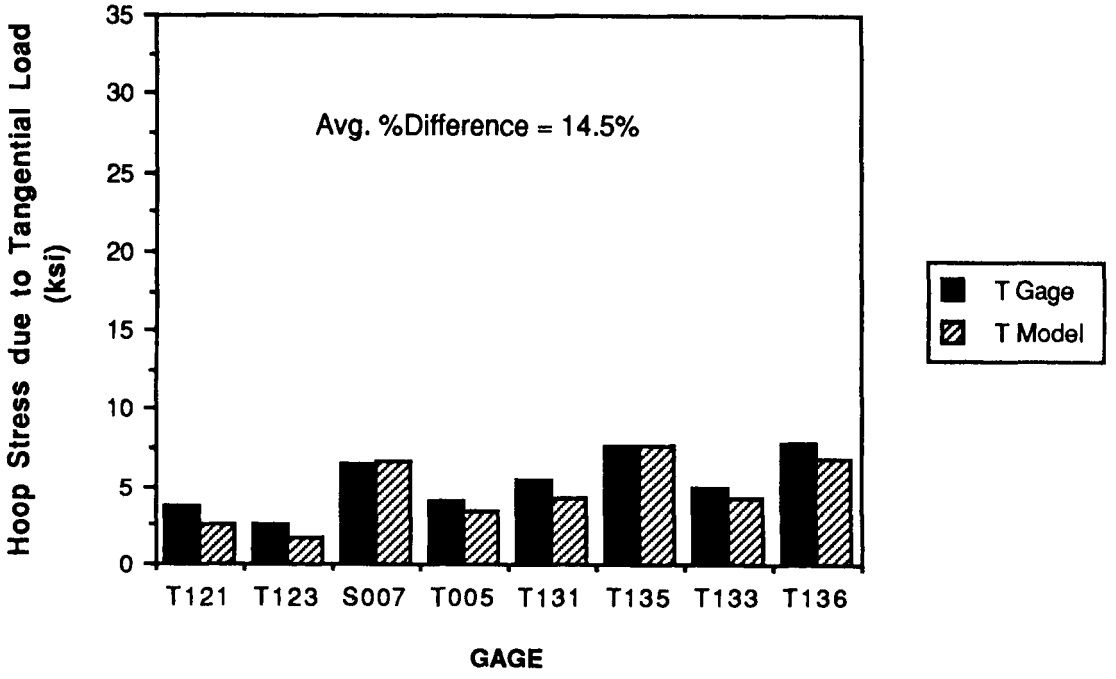

Figure 9. Strain Gage Correlation for Tangential Applied Load

Table 5. STRAIN GAGE CORRELATION SUMMARY

	+ R LOAD			+ T LOAD			+Z LOAD		
	GAGE	MODEL	% DIFF	GAGE	MODEL	% DIFF	GAGE	MODEL	% DIFF
T121	20.3	18.4	-9	3.8	2.6	-32	15.2	14.6	-4
T123	14.2	12.5	-2	2.6	1.7	-35	10.8	10.0	-7
S007	28.4	30.4	+7	6.5	6.6	+2	21.6	23.8	+9
T005	18.1	5.5	-9	4.1	3.4	-17	13.6	13.0	-4
T131	18.0	7.5	-3	4.5	4.3	-4	13.9	13.4	-4
T135	29.0	29.0	0	7.7	7.6	-1	22.0	22.0	0
T133	16.9	16.0	-5	4.9	4.3	-12	13.4	12.3	-9
T136	25.0	23.0	-8	7.9	6.9	-13	19.6	7.4	-11
AVG			6.6			14.5			5.9
MAX			12.0			35.0			11.0
MIN			0.0			1.0			0.0

4. REDESIGN ANALYSIS

4.1. BRIEF DESCRIPTION OF REDESIGN

The redesign of the Aft Skirt was limited to the aft ring bracketry. This bracketry was increased in size to add strength to the post to skin weld area. Figure 10 shows the original design, and Figure 11 the redesigned configuration.

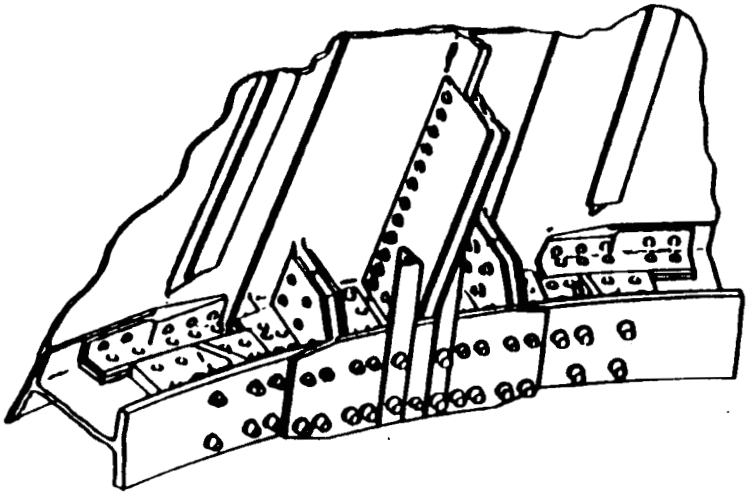

HOLDDOWN POST/AFT RING AREA
UPPER VIEW (EXISTING DESIGN)

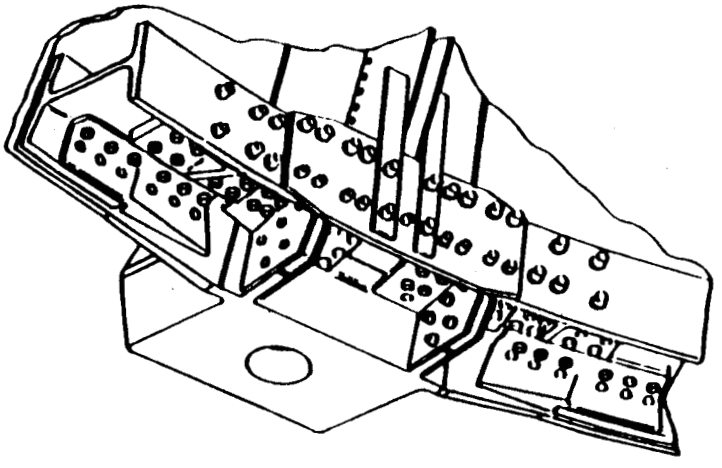

HOLDDOWN POST/AFT RING
BOTTOM VIEW (EXISTING DESIGN)

Figure 10. Original Aft Ring Bracketry

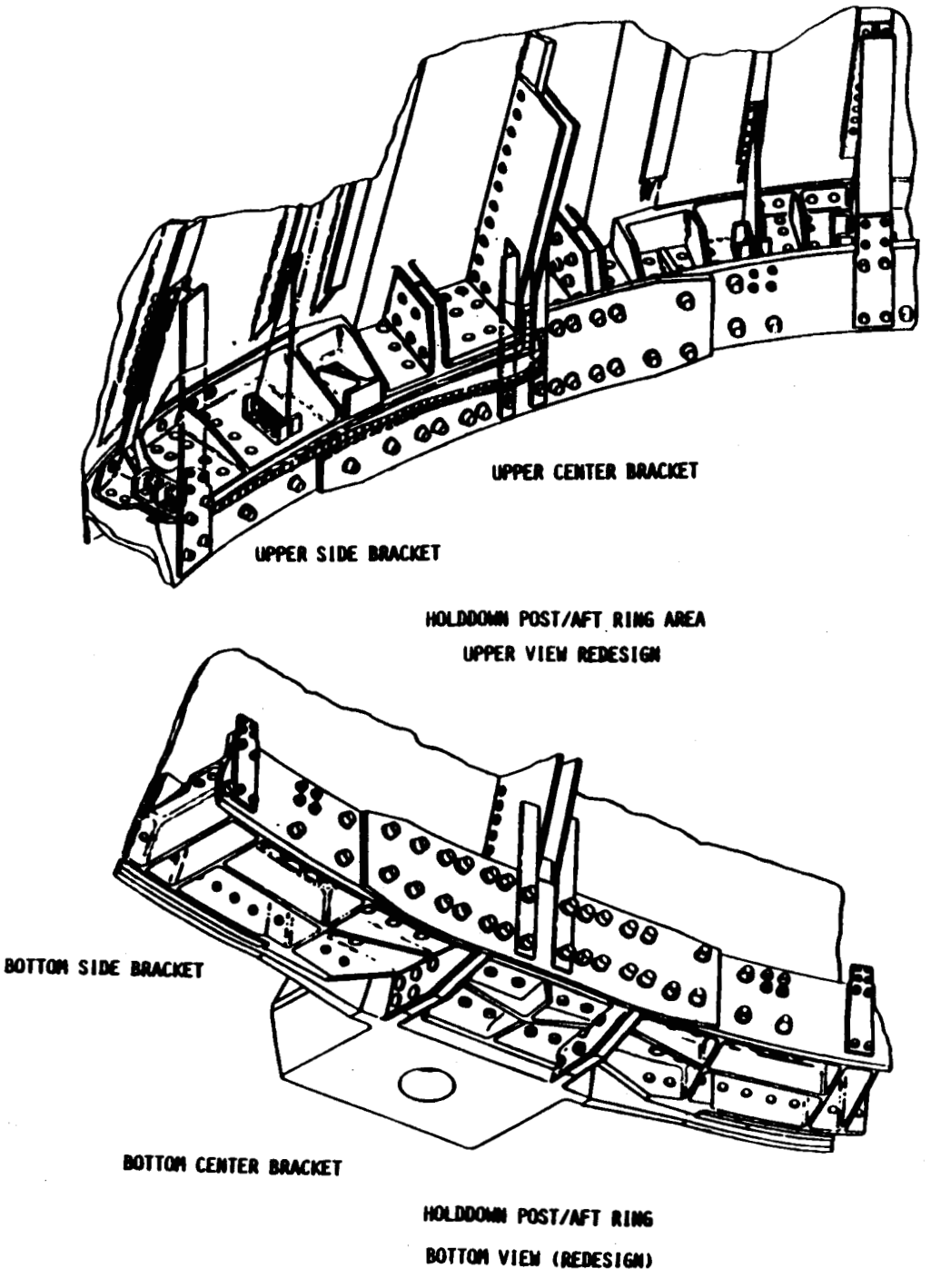

Figure 11. Redesigned Aft Ring Bracketry

4.2. GLOBAL MODEL REDESIGN

4.2.1. Modeling Procedure

To incorporate the redesign into the existing finite element models, the current models were copied from the MSFC IBM to the Lockheed HEC VAX computer. ANSYS was installed on the HEC VAX in October, 1987 and was used to incorporate the redesign. Several HEC personnel were assigned various parts of the redesign, Robert Shannon and David Berry the skin sections, Gregory Sisk the upper post sections, and Mark Stansberry the lower post sections. Elements relating to the original design but not present in the redesign were identified and deleted along with their corresponding nodes. Only the original aft-ring, forging, and skin portions from the original model were used in the redesign of the structure. Each person modeling a portion of the redesign was assigned a node range with which to work, using care not to include existing node numbers. For example, the upper portion of the post sections was assigned a unique node range different from the lower portion of the redesigned post section. Once a post section was completed, the other post section was modeled simply by taking the nodes and elements in the completed redesign portion, incrementing the node numbers to the assigned range, and translating the nodal coordinates to coincide with the appropriate post. Nodes were then merged to connect the redesigned structure to the post. The skin sections were completed in a similar manner.

4.2.2. Resulting Sizes and Changes to Model

The redesigned global model has approximately the same number of nodes and elements as the original design, only higher node numbers. The basic dimensions and geometric characteristics remain the same.

4.2.3. Execution Procedure

The solution procedure is the same as for the original design, except that a solution-only version of ANSYS was installed on the MSFC Cray. This required all post- and preprocessing to be done on the IBM front end processor. For a normal static solution, this constraint ordinarily poses no major problems. The problem at hand, though, called for manipulating large files between the Cray and IBM and essentially doubling the number of runs required. The primary difficulty was acquiring enough disk space on the IBM to store the large files.

Substructure generation runs were made on all redesigned substructures. Also, the use pass was performed to obtain displacements at the substructure boundaries for the redesigned structure. Stress passes could be executed on either the original or redesigned structure by using the appropriate files corresponding to a particular configuration.

4.3. DETAILED MODEL

Because no portions of the redesign were in the detailed model, no changes were required to the existing model.

The solution of the detailed model with the redesign boundary conditions was basically the same. The only exception was the solution-only version of ANSYS installed on the Cray. This required performing the cut boundary interpolation portion of the analysis on the IBM. A linear stress run was then executed, and reaction forces were obtained. These forces were used as boundary conditions in a nonlinear analysis execution on the Cray.

4.4 RELATIVE INFLUENCE OF LOADS APPLIED TO EACH POST

During the analysis, a question arose: how did each component of load applied to the Aft Skirt affect the stress in the failure region. If this were known, assuming the stresses combined linearly, each load case could be evaluated to determine the overall worst load case. The ANSYS global model was executed for 12 load cases, one for each post in each direction. A 1000 -lb load was applied in each load case. The results show the hoop stress in the failure region due to each "unit" load. These results, shown in Table 6, can be used to derive an equation to predict which load case will cause the highest linear hoop stress in the failure area.

4.5. RESULTS (PRIOR TO STA-3 TEST)

The detailed nonlinear model of the Aft Skirt failure area was executed for the redesigned configuration for both STA-2B and STA-3 loads. The equivalent plastic strain on

Table 6. FAILURE AREA HOOP STRESSES DUE TO UNIT LOADS

1K LOAD APPLIED ONLY ON		HOOP STRESS (psi)			
POST	DIRECTION	@ Post 5	@ Post 6	@ Post 7	@ Post 8
POST 5	RADIAL	194.5	-45.8	4.9	11.3
	THETA	46.495	12.3	10.175	0.79
	AXIAL	-75.79	20	-2.98	-4.93
POST 6	RADIAL	-41.94	208.5	13.32	6.5
	THETA	-12.915	-46.5	-0.865	-9.5
	AXIAL	18.06	-80.9	-5.94	-3.8
POST 7	RADIAL	4.9	11.3	194.5	-45.8
	THETA	-10.175	-0.79	-46.495	-12.3
	AXIAL	-2.98	-4.93	-75.79	20
POST 8	RADIAL	13.32	6.5	-41.94	208.5
	THETA	0.865	9.5	12.915	46.5
	AXIAL	-5.94	-3.8	18.06	-80.9

the outside surface of the model and on a cross section of the weld is shown in Figures 12 and 13, respectively. When compared to the analysis of the original design (STA-2B loads applied) the following results were obtained.

(1) When STA-2B loads were applied, the equivalent plastic strain in the fillet area decreased 45% in the redesign.

(2) When STA-3 loads were applied, the equivalent plastic strain in the fillet area decreased 43% in the redesign.

(3) When STA-2B loads were applied, the equivalent plastic strain in the HAZ decreased 43% in the redesign.

(4) When STA-3 loads were applied, the equivalent plastic strain in the HAZ decreased 51% in the redesign.

These results along with results from the global model are detailed in Table 7.

The most significant results of this analysis are shown in Figure 14. This figure shows the percentage of plastic strain in the HAZ versus the percentage of limit load for the different load cases and designs. The uppermost curve shows the original design STA-2B analysis results, which predicted 1.4% equivalent plastic strain in the HAZ at 129% of limit load. The lowermost curve shows the original design STA-1 analysis results, which predicted a much lower equivalent plastic strain of 0.4%. Even though the curve

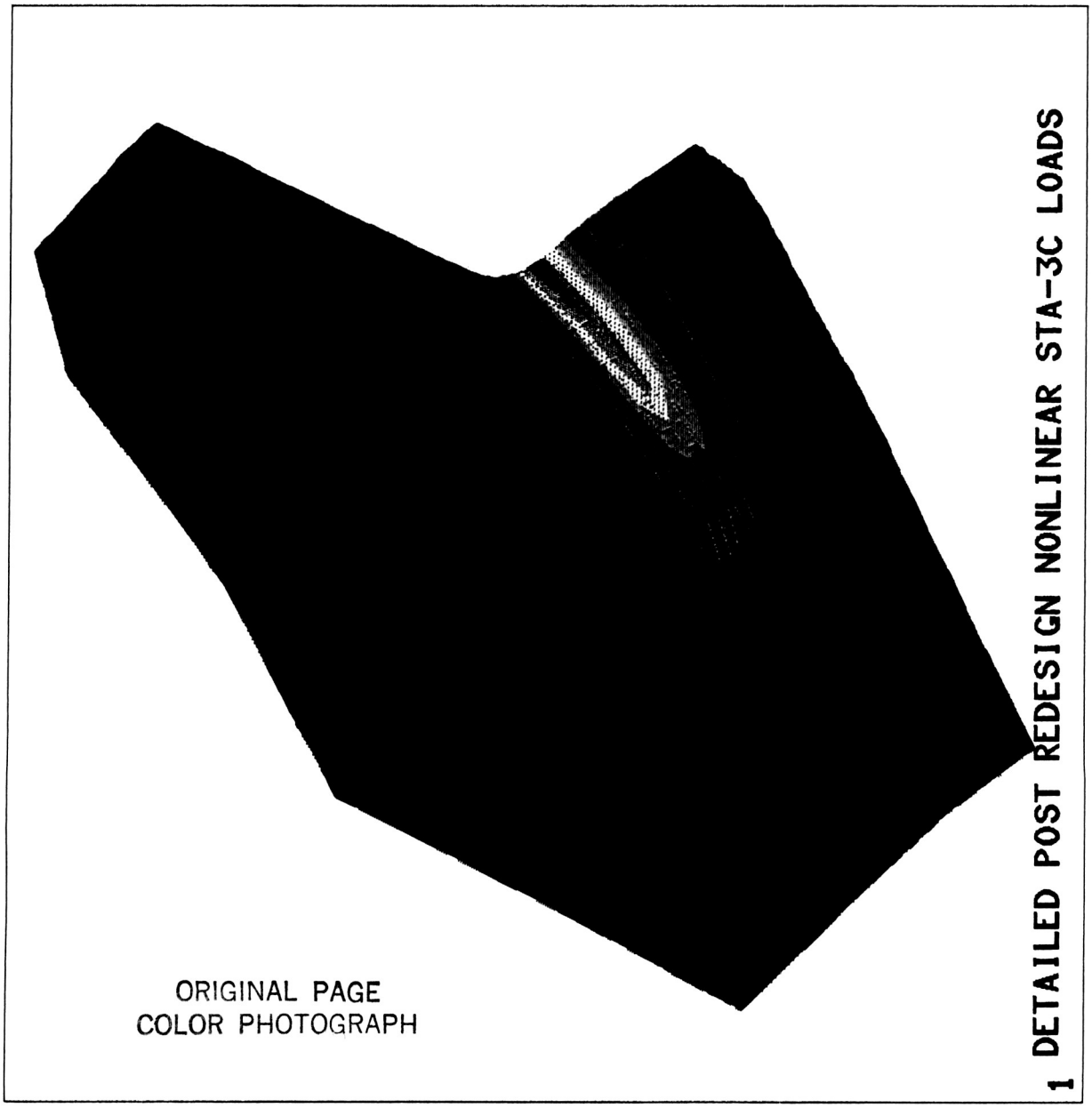

Figure 12. Equivalent Plastic Strain (STA-3, Redesign)

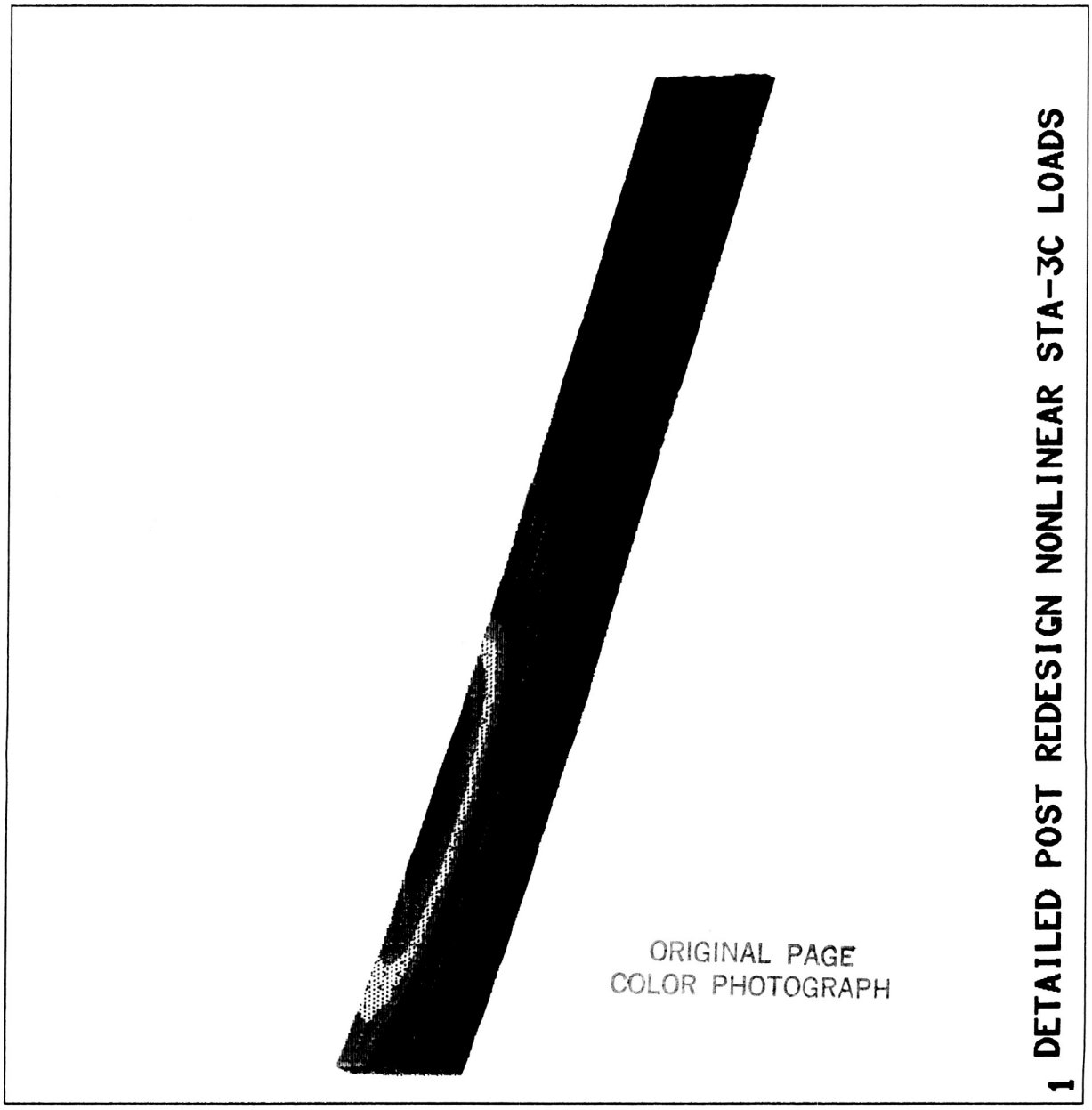

Figure 13. Equivalent Plastic Strain in HAZ (STA-3, Redesign)

Table 7. PRETEST ANALYSIS: REDESIGN VERSUS ORIGINAL DESIGN

	GLOBAL MODEL		DETAILED MODEL		
			LINEAR	NONLINEAR	
	Tangential Stress (ksi)	Max Principal Stress (ksi)	Max Principal Stress (ksi)	Equivalent Plastic Strain (% Strain)	
				Fillet Area	Weld Material
Original Design STA-1		46	80	0.61	0.38
Original Design STA-2B	52	54	101	1.70	1.40
Redesign STA-2B (*)	46 -12%	46 -15%	92 -09%	0.94 -45%	0.80 -43%
Redesign STA-3 (*)	45 -13%	50 -07%	95 -06%	0.97 -43%	0.68 -51%

* = Difference from Original Design STA-2B Loads

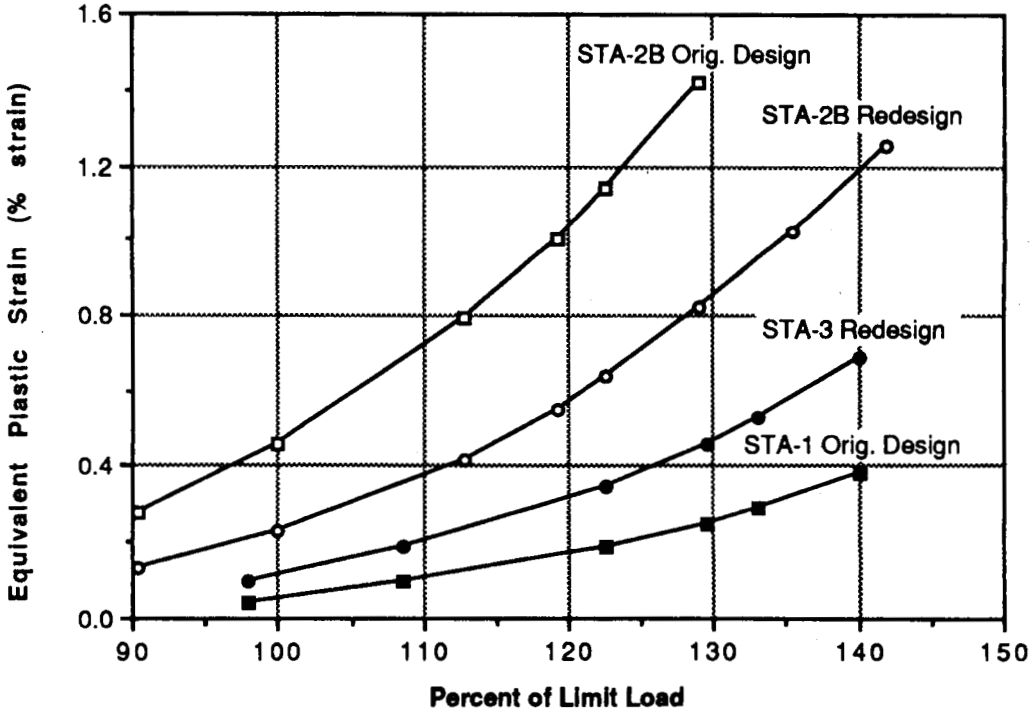

Figure 14. HAZ Plastic Strain (Original versus Redesign)

representing the redesign STA-3 analysis results shows 0.7% plastic strain, it is significantly lower than the STA-2B curve. In sum, this figure shows the nonlinear behavior which causes the large differences in strains due to different load cases, even though the load cases may appear similar in linear analyses.

There are four strain gages in the portion of the Aft Skirt described by the nonlinear detailed model. Predictions of the strains that will be measured by these gages during the STA-3 test were derived from the finite element model. These are given in Figure 15.

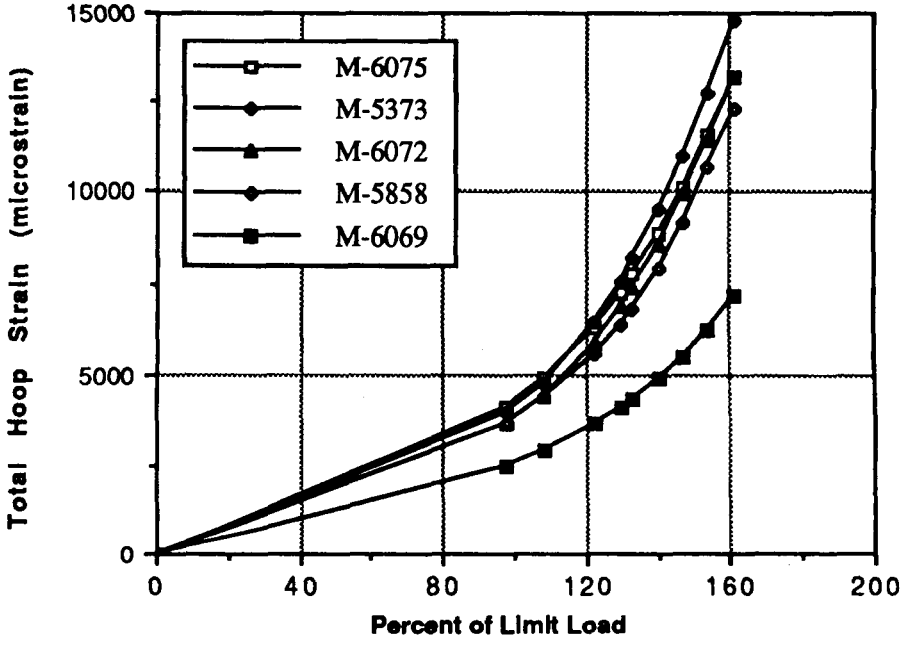

Figure 15. Predicted Hoop Strain versus Load for STA-3 Gages

5. STA-3 FAILURE INVESTIGATION

5.1. INTRODUCTION AND TEST RESULTS

Lockheed HEC personnel monitored the post 8 strain gages during the STA-3 test. The pretest analysis tracked the gages in the post 8 weld region very well up through the last recorded data point. However, the post 8 weld failed at approximately 132% of limit load. This is below the expected load carrying ability of the Aft Skirt and appears to be contradictory to the strain gage values which showed less than 0.8 % strain in the weld area. This prompted a thorough review of the pretest predictions and a comparison of the pretest predictions to STA-3 test data.

Results of the analysis to date were presented to the Burridge committee on 24 May 1988. Most of the STA-3 failure investigation portion of this report was presented to the committee at that time.

5.2. COMPARISON OF PRETEST PREDICTIONS WITH STA-3 TEST RESULTS

The pretest predictions, as presented at the Test Readiness Review, were as follows:

(1) The redesigned Aft Skirt acted on by STA-3 loads experiences a 43% decrease in equivalent plastic strain in the forging fillet area when compared with the original design Aft Skirt acted on by STA-2B loads.

(2) The redesigned Aft Skirt acted on by STA-3 loads experiences a 51% decrease in equivalent plastic strain in the HAZ when compared with the original design Aft Skirt acted on by STA-2B loads.

The predicted total hoop strain for each of four gages in the failure region is compared with the actual strain gage measurements in Figures 16 through 19. These plots show that the pretest analysis tracked the gages in the post 8 failure region very well up through the last recorded data point.

During the STA-3 test, gage T6072 at the aft ring centerline consistently measured strains 40% below a gage located at approximately the same position during the STA-2B test. This compares with the 51% reduction predicted in the pretest analysis.

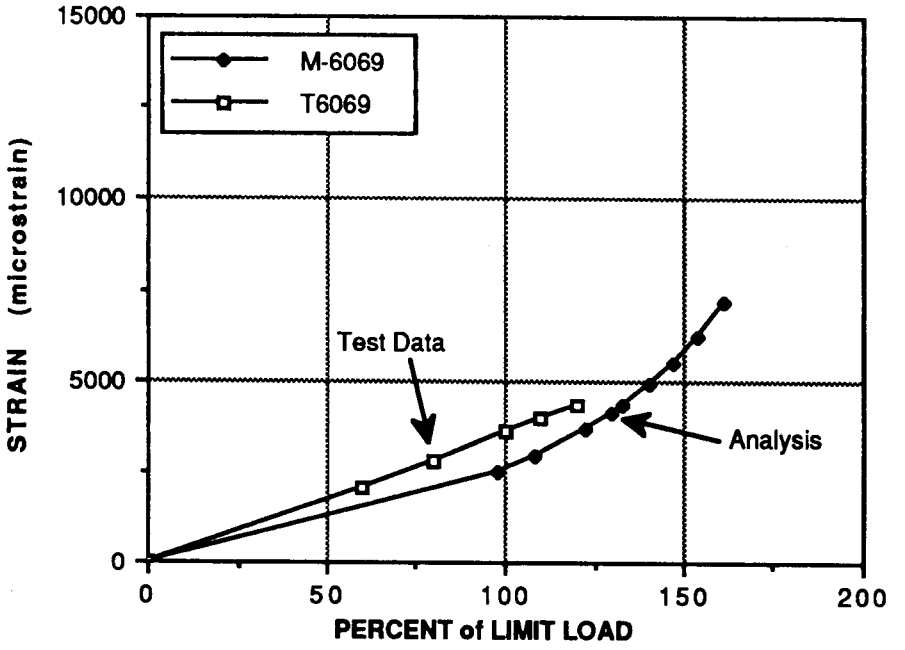

Figure 16. STA-3 Test versus Analysis (Gage T6069, Z = 7.42 in.)

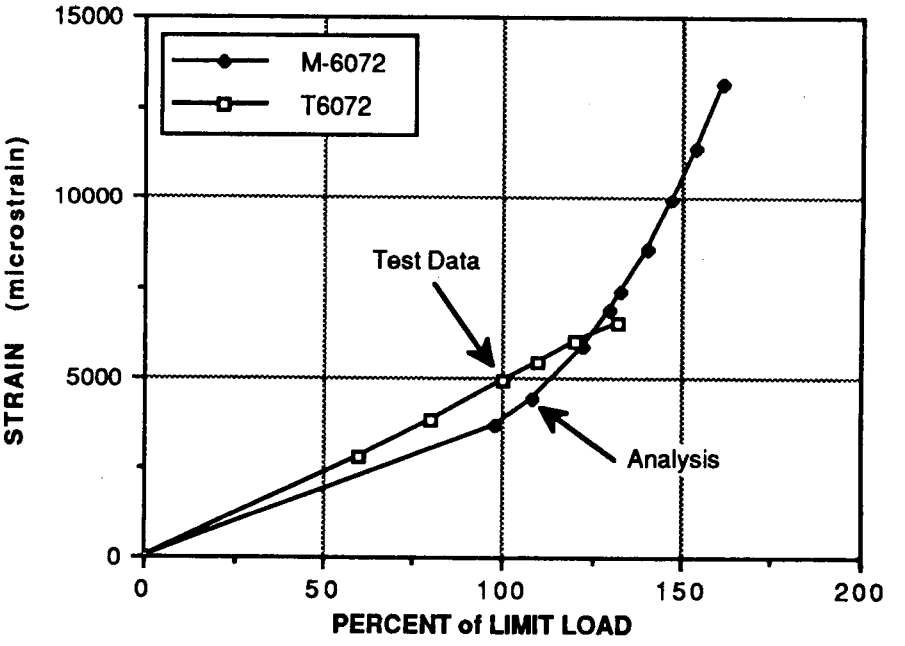

Figure 17. STA-3 Test versus Analysis (Gage T6072, Z = 4.42 in.)

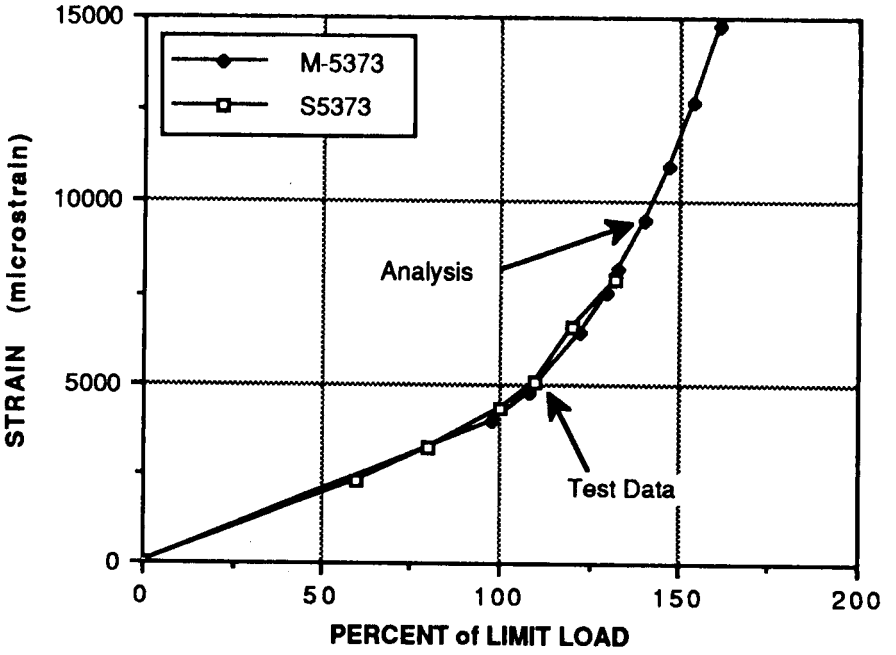

Figure 18. STA-3 Test versus Analysis (Gage S5373, Z = 2.21 in.)

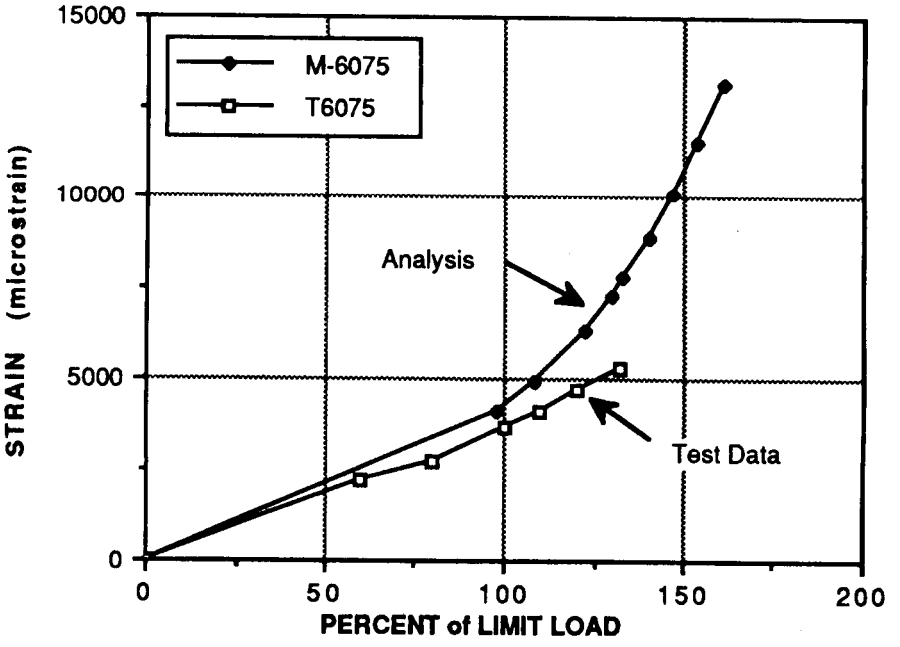

Figure 19. STA-3 Test versus Analysis (Gage T6075, Z = 0.25 in.)

5.3. POST-TEST ANALYSIS

5.3.1. Use of Pretest (Minimum) Properties

It has been suggested that the softer and weaker heat affected material lies in a thin (0.2 in.) band along the weld line and that, therefore, the strain gages, which were located 0.5 in. from the weld centerline, did not detect the high strains in this region.

The detailed nonlinear finite element model shows higher strains in the weld than at the gage locations in the area between 3.5 and 6.0 in. from the bottom of the post. It is in this area that the weld is closest to the post. However, the analysis predicts only a 13% increase in total strain between the gage location (0.8% strain) and the weld (0.9% strain) at 140 % of limit load. This is shown in Figure 20 as a plot of total hoop strain per element as the element location proceeds from the post fillet toward the weld.

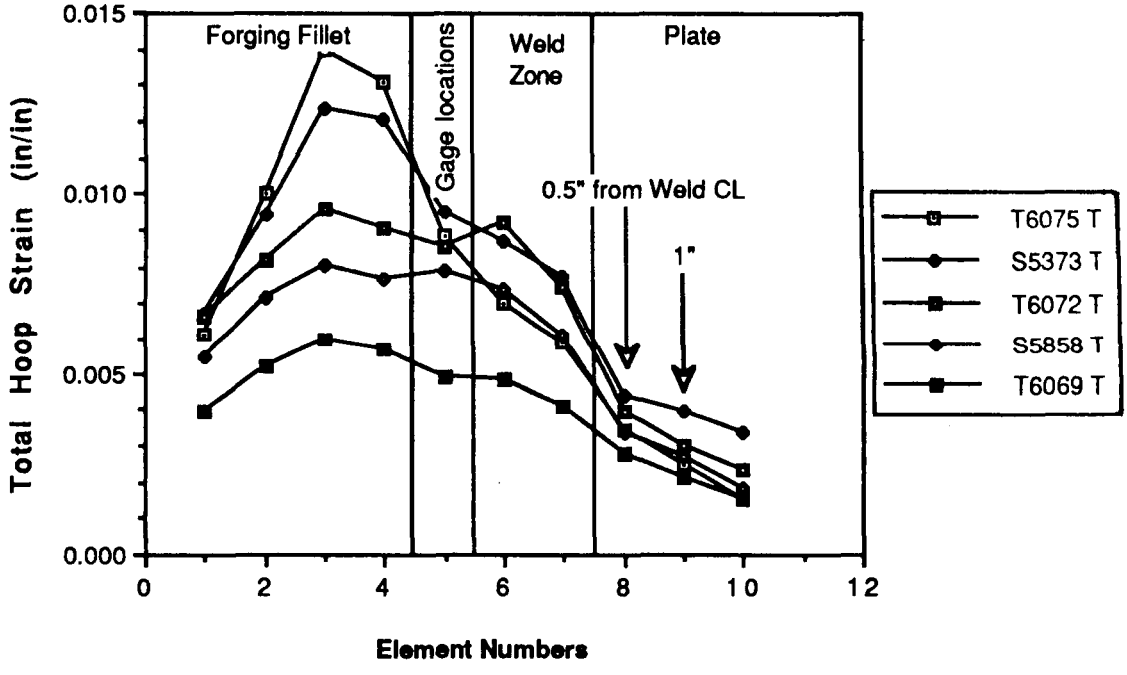

Figure 20. Pretest Prediction at 140% of Limit Load

5.3.2. Using Post-Test (Typical) Properties with Refined Model

The detailed finite element model has been further refined to include the thin bands of different material properties that lie in the weld area and to use typical forging properties. This refined detailed model is shown in Figure 21. The model now contains separate material properties for each of the following: forging parent material, forging HAZ, weld/forging interface, weld center, weld/plate interface, plate HAZ, and plate parent material. The new forging and forging heat affected properties are compared to the forging and weld properties used in the pretest analysis in Figure 22.

Figure 22 shows that both the new forging and new forging HAZ materials are stiffer than the corresponding materials in the pretest model. The difference in stiffness between the materials is greater in the post-test model than in the pretest model.

Figure 23 is a plot of total hoop strain per element as the element location proceeds from the post fillet toward the weld (similar to the sequence in Figure 20 for the pretest analysis). The results shown in this figure could be inferred from Figure 22. Due to the increased stiffness, the magnitudes of the strains are lower and, like the stiffnesses, the difference in strain between the HAZ (0.6% strain) and the weld (0.8% strain) is greater.

Figure 24 shows the equivalent plastic strain at a maximum at the interface between the forging parent material and the forging HAZ. Figure 25 shows the total hoop strain in the HAZ.

5.3.3. Parametric Study of Material Properties

The nonlinear detailed model of Aft Skirt with the refined weld area has been executed with modified material properties. The modification was made by replacing the thin band of typical forging HAZ properties used in the post-test analysis with the minimum weld properties used in the pretest analysis.

The pretest properties are softer than the typical properties as shown previously in Figure 23. The elements of the finite element model affected by this change lie in a thin band at the edge of the weld area.

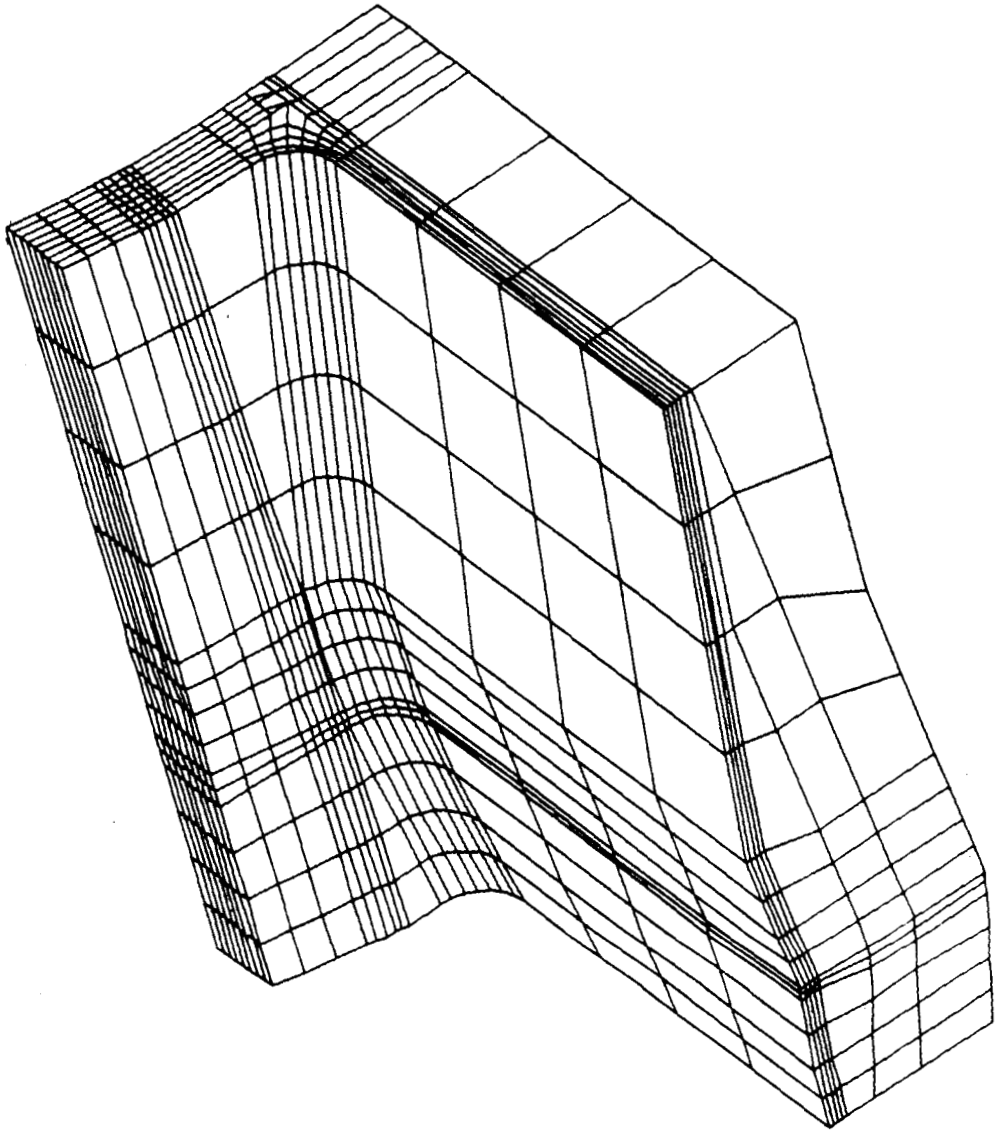

Figure 21. Refined Model Used in Post-Test Analysis

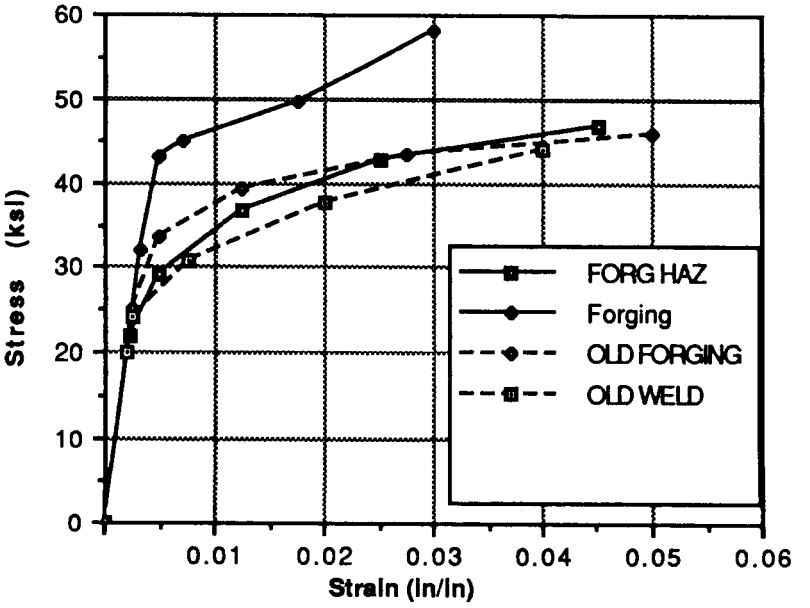

Figure 22. Pretest versus Post-Test Material Properties

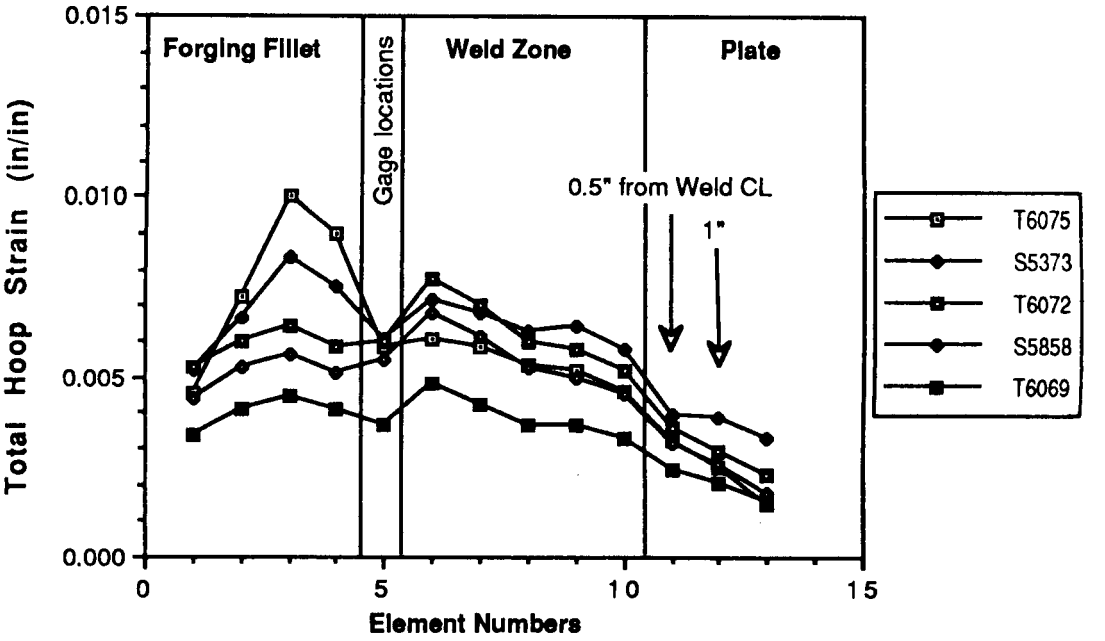

Figure 23. Post-Test Analysis (140% Limit, Typical Properties)

Figure 24. Equivalent Plastic Strain (Redesign, Typical Properties)

ORIGINAL PAGE
COLOR PHOTOGRAPH

Figure 25. Total Hoop Strain in HAZ (Redesign, Typical Properties)

The results of this analysis are shown in Figure 26 as a plot of total hoop strain per element as the element location proceeds from the fillet through the weld area. The effect of the property change in the thin forging HAZ is very slight. The total hoop strain increase (compared to analysis using typical properties) in the forging HAZ area is only 0.02% strain. This increase is negligible and indicates that a larger change in properties and/or a change over a wider area would have to occur for the model to predict significantly larger strains in the forging HAZ.

5.4. TEST SPECIMEN MODELS

To better understand the material behavior of the forging-plate weld, an ANSYS nonlinear finite element modelwas constructed. Material properties, furnished by the Materials Laboratory at MSFC, varied every 0.125 in. in the weld zone. Figure 27 shows the material properties used. Figure 28 shows how the material properties were divided along the length of the bar. The model was a 7/8 x 7/16 in. bar 2.68 in. long, with symmetry boundary conditions applied to simulate a 7/8 in. square bar used during testing.

Three separate load cases were evaluated. First, a tension load of 45,000 psi was applied. During the analysis, load was gradually applied to reach the desired endpoint. A solution was performed at each load, iterating until a converged solution was obtained. Viewing results from each of these load steps showed that the maximum strain initially begins in the forging HAZ. This is because the forging HAZ is the softest material and starts yielding before the other materials. Further loading causes a shift in the location of the maximum strain towards the center of the weld material. Initially, the cause of this concentration was believed to be a Poisson effect. Several additional runs were made varying Poisson's ratio in the material, with insignificant changes in the results. One possible explanation is that, as loads are increased, the softer HAZ material is partially constrained by the harder forging material due to its proximity. This phenomenon was also observed in the bending and tension plus bending models. At 50% load, the maximum strain is 0.228% in the forging HAZ. When the load level reaches 70% of 45 ksi, the maximum strain is 0.497%, concentrated in the weld. At this point, there are still some comparable strains in the forging HAZ. At 90% load, all the maximum strain range is concentrated in the center of the weld with a maximum of 1.49%. At 100% load, the maximum strain of 2.54% is in the center of the weld. Figure 29 depicts the tension model

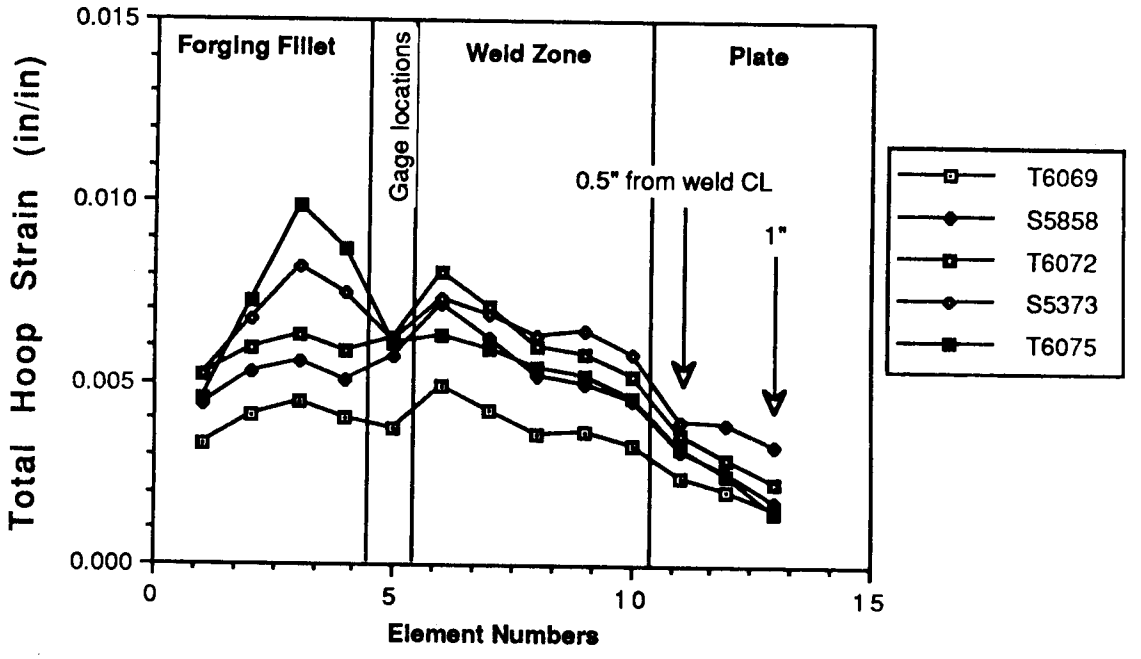

Figure 26. Predicted Strain at 140% Limit Load with Material Modification

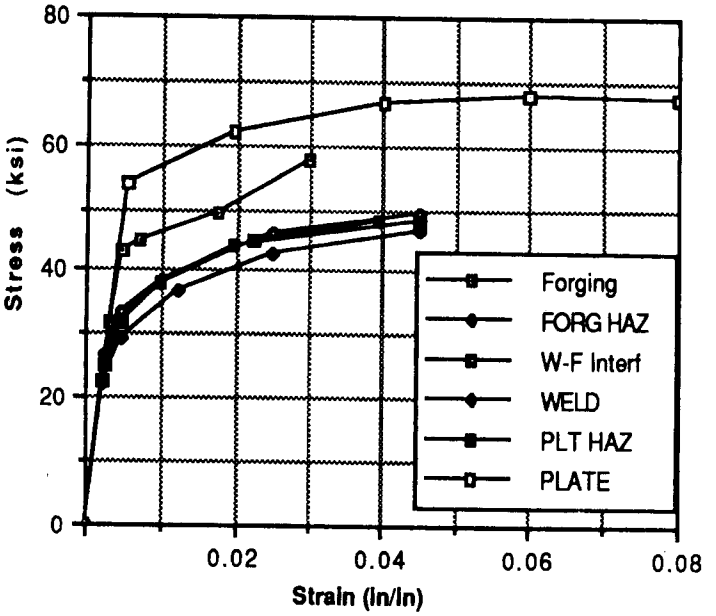

Figure 27. Material Properties Used in Test Specimen Model

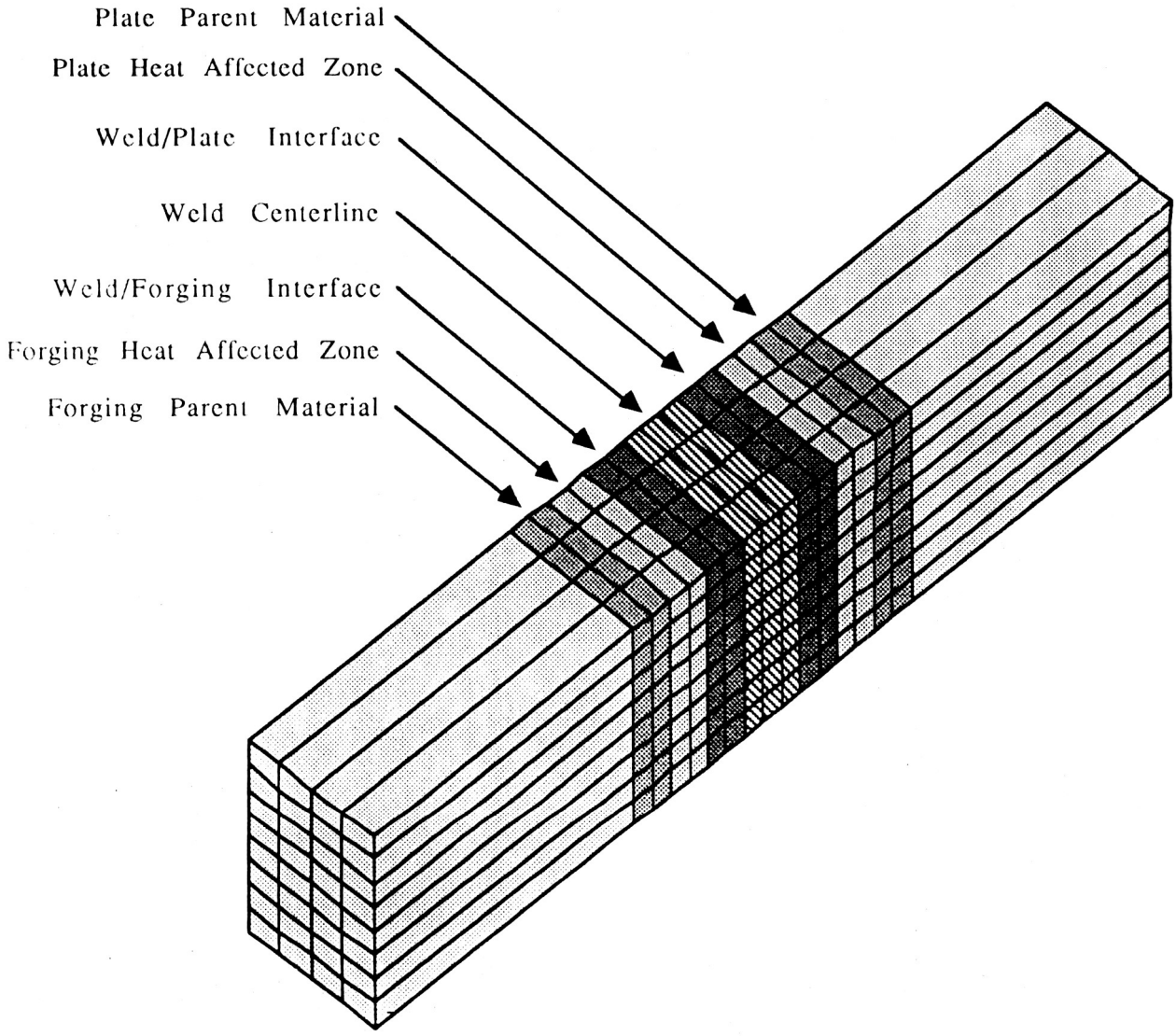

Figure 28. Test Specimen Model Showing Bands of Nonlinear Materials

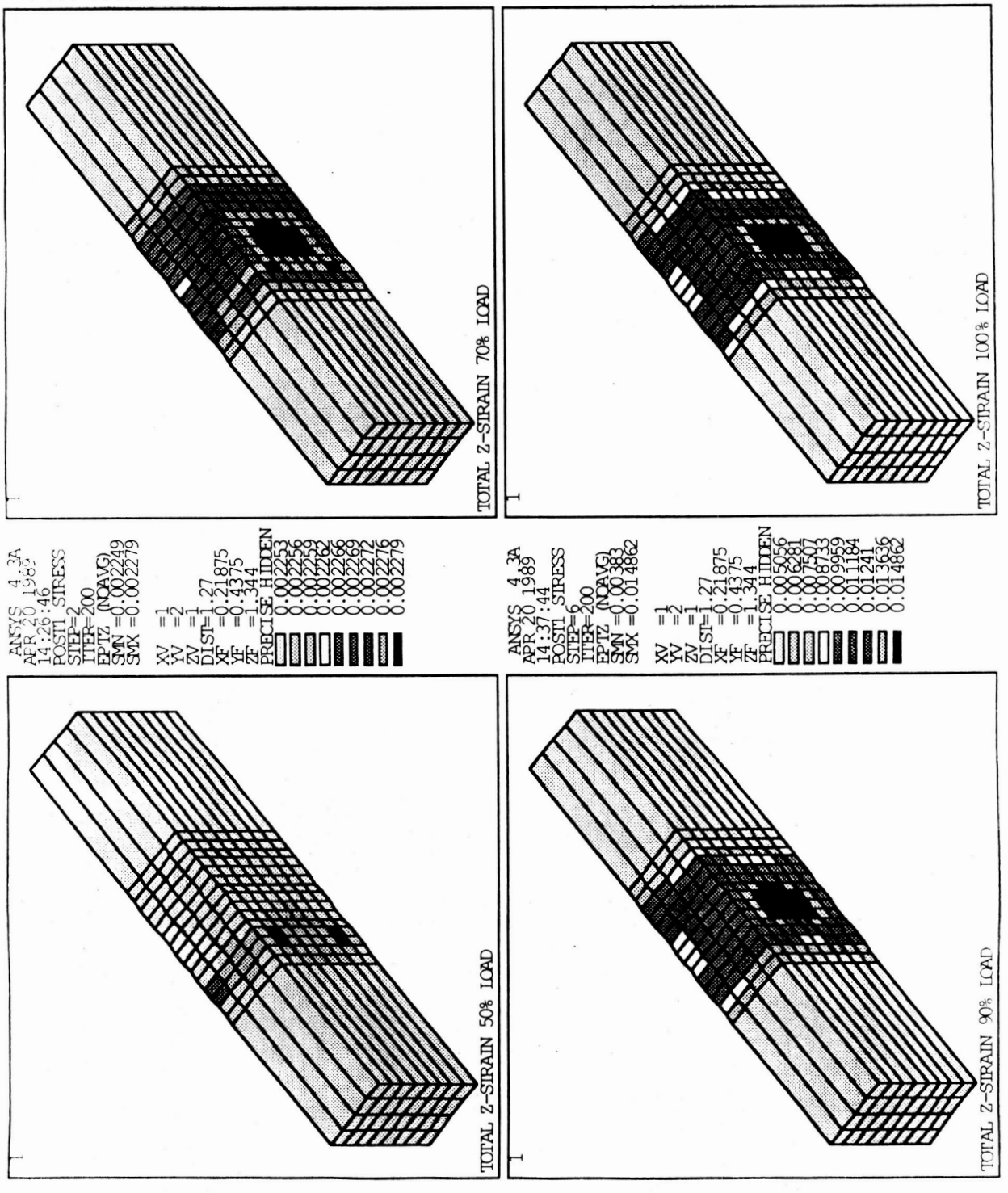

Figure 29. Strains Induced by Tension Load on Specimen Model

at various stages of loading. Strains measured during the tension test were slightly higher than those seen in the analysis. However, at the load levels tested, small increases in applied load result in substantial elevations in strain. For example, Figure 30 shows the tension model at 105% of the 45,000 psi load. For this 5% increase in load, the maximum strain is 3.64%, an increase of 43%.

Second, a bending load was applied by varying the pressure on the end from -37,500 to +37,500 psi. Again, initially the greatest strains were in the forging HAZ but migrated towards the center of the weld as loads were increased. At 50% of bending load, the maximum strain of ±0.175% is in the outer fibers of the forging HAZ. At 70% load, the maximum strains are still in the outer fibers of the forging HAZ. By 90% load, the maximum strain of ±1.7% is almost centered about the weld material outer fibers, but now extends to both the forging and plate HAZ materials. At 100% load, the maximum strains are concentrated about the weld element outer fibers and have values of ±2.75%. Figure 31 shows the bending model at various stages of loading.

Last, a tension plus bending load was applied using a pressure varying from 0 to 67,500 psi. At 50% load, the maximum strain of 0.48% is located in the forging HAZ. At 70% load, the maximum strains have shifted towards the weld but still remain in the forging HAZ material. The maximum strain is 2.99% at 90% load. The maximum strains are now concentrated about the weld material outer fiber, but extend to the HAZ materials. At 100% load, the maximum strain is 5.58%. One element in each of the HAZ materials is strained in the maximum range. Figure 32 shows the tension plus bending model at various stages of loading.

The analysis showed that strains in the weld interface materials did not possess the maximum strains at load levels significantly above yield. Strain peaking at the forging HAZ did not appear as test data, although, depending on gage placement, an increase could be manipulated. The analysis also revealed substantial variations in strain through the thickness of the specimen. Hand analysis using textbook plasticity equations assumes that plane sections remain plane. However, this assumption breaks down as load levels are increased beyond yield, as evidenced by Figure 33. This graph depicts strain variations through the thickness of the specimen which would be flat if plane sections remained plane.

Figure 30. Strains Induced by 105% of Tension Load

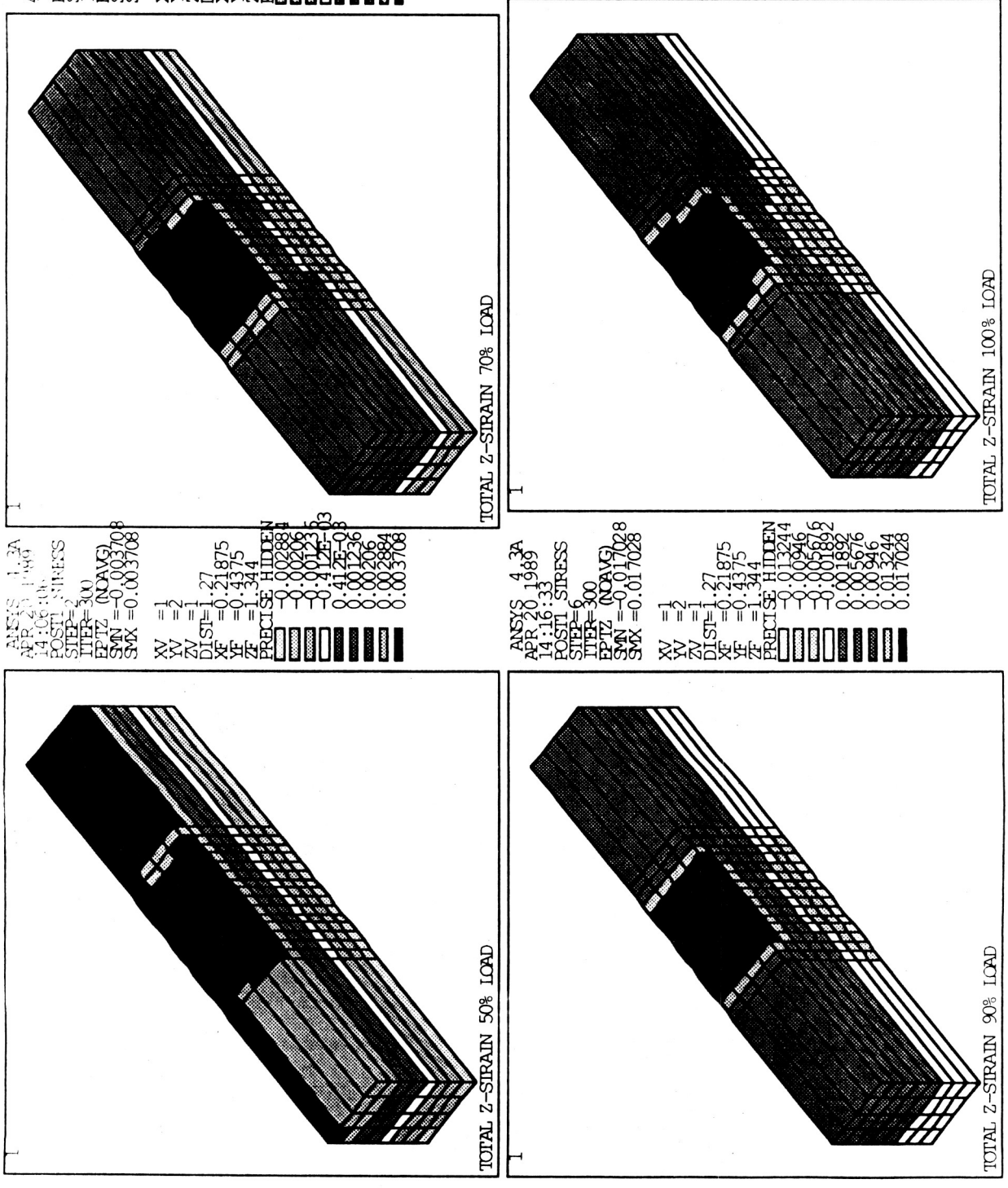

Figure 31. Strains Induced by Bending Load on Specimen Model

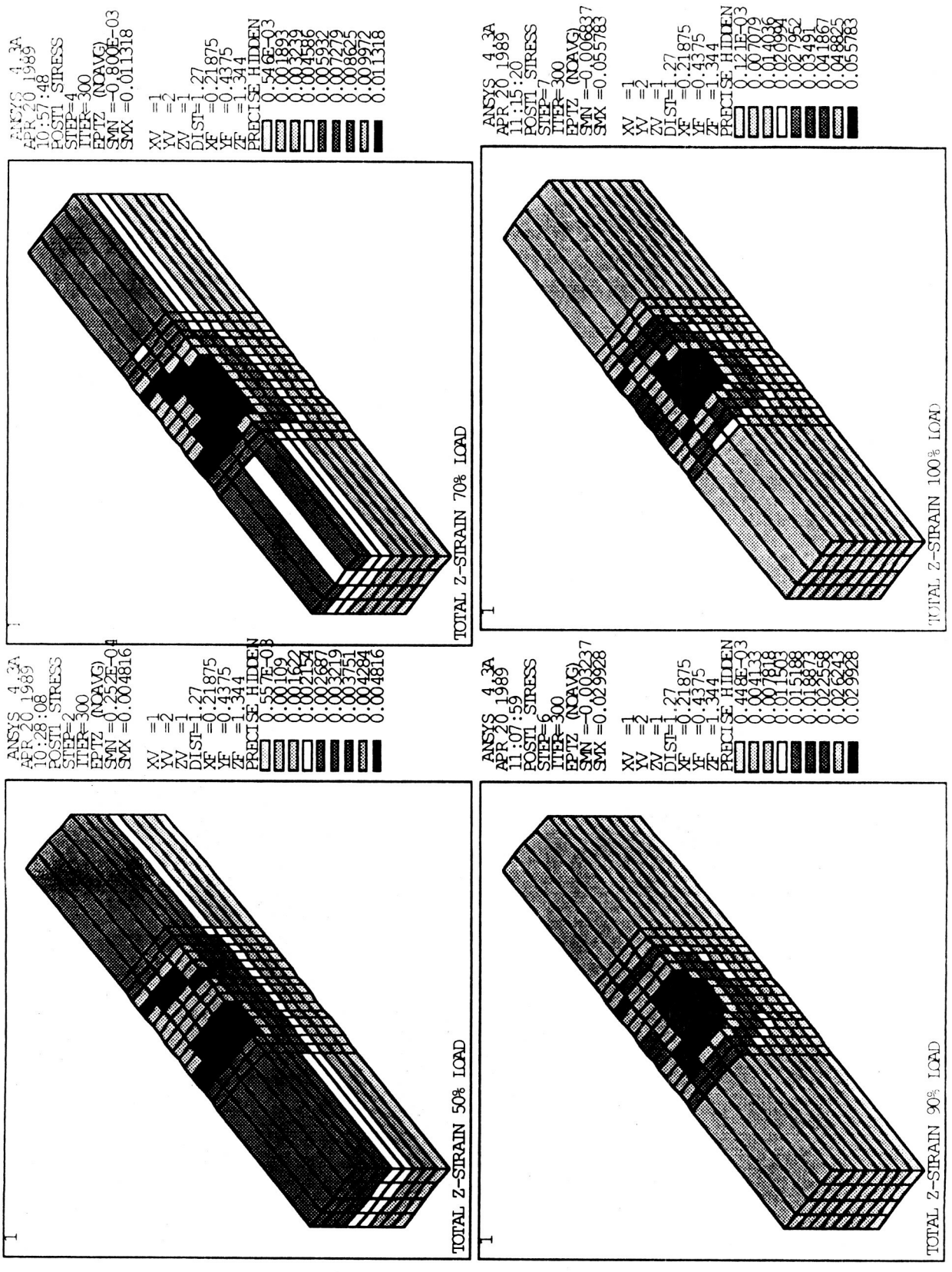

Figure 32. Strains Induced by Combined Load on Specimen Model

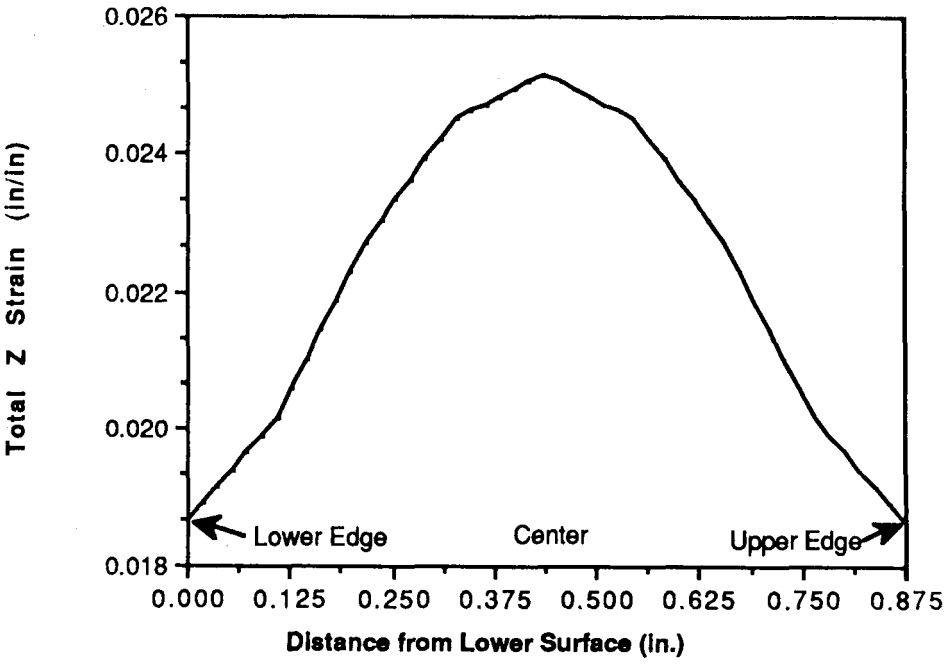

Figure 33. Strain Profile of Specimen Model under Tension Load

5.5. COMPARATIVE STUDY OF POSTS 7 AND 8

Holddown post 7 has been analyzed in an attempt to explain apparent differences in the behavior of posts 7 and 8. This analysis was accomplished using a mirror image of the post 8 detailed model in a nonlinear analysis. This model uses the stiffer typical material properties used previously in the post-test analysis model. Boundary conditions were obtained from the post 7 region of the ANSYS global finite element model.

Figures 34 through 37 show the predicted strains versus load for post 7 at four strain gage locations compared to the predicted post 8 strains at corresponding strain gage locations.

The analytical models of posts 7 and 8 behave very similarly, with the strains at the four gage locations on post 7 essentially matching the strains of the equivalent locations on post 8 (within 0.1 % strain). Figure 35 shows that the predicted strains at the aft ring centerline location on posts 7 and 8 are extremely close.

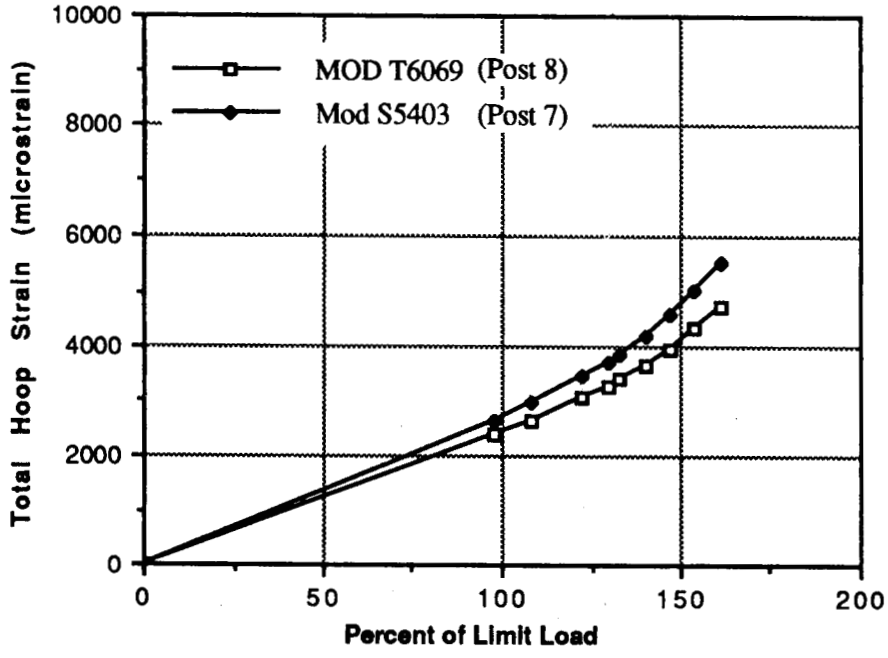

Figure 34. Predicted Strains at T6069 and T5403 (Z = 7.42 in.)

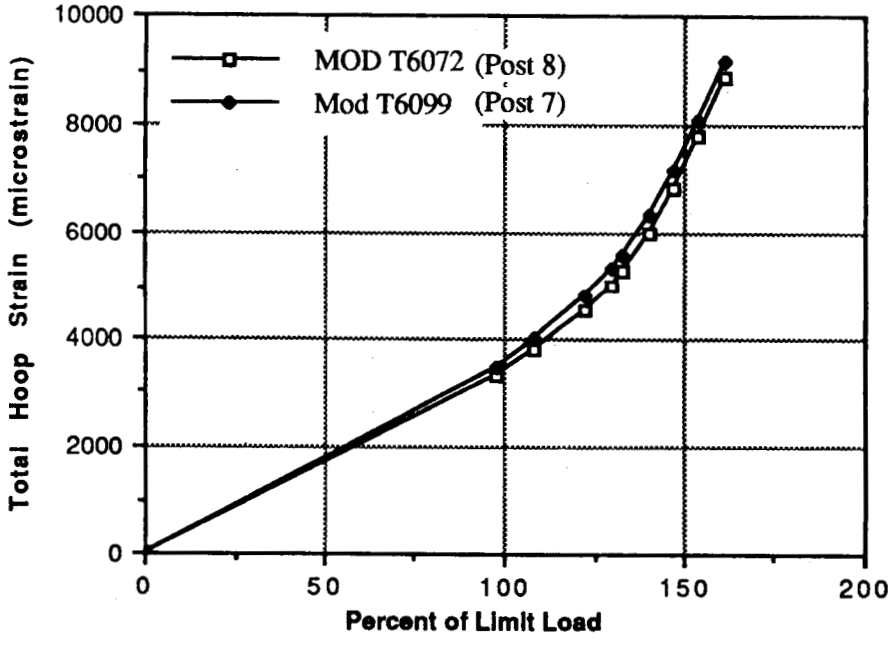

Figure 35. Predicted Strains at T6072 and T6099 (Z = 4.42 in.)

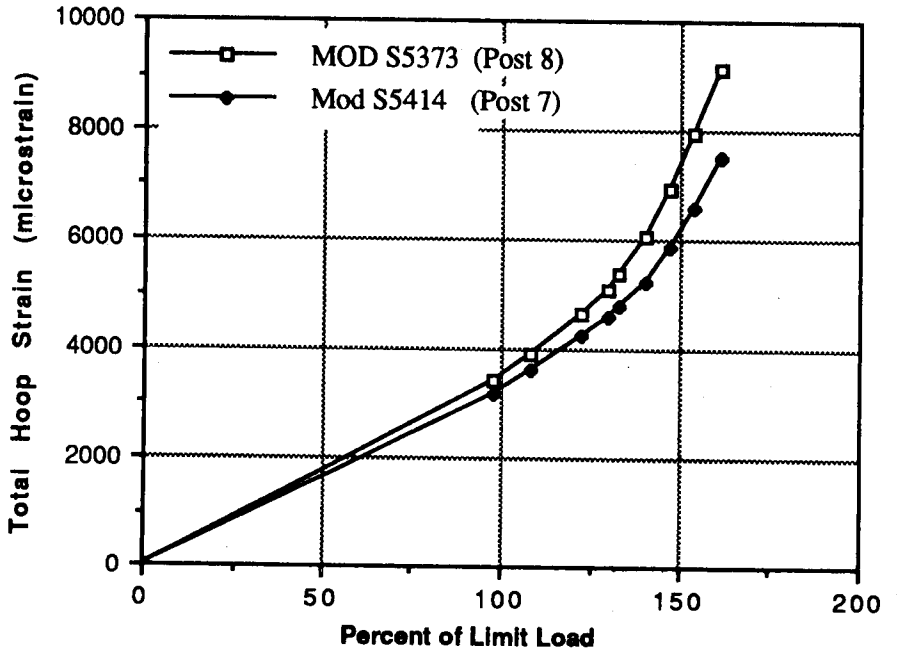

Figure 36. Predicted Strains at S5373 and S5414 (Z = 2.21 in.)

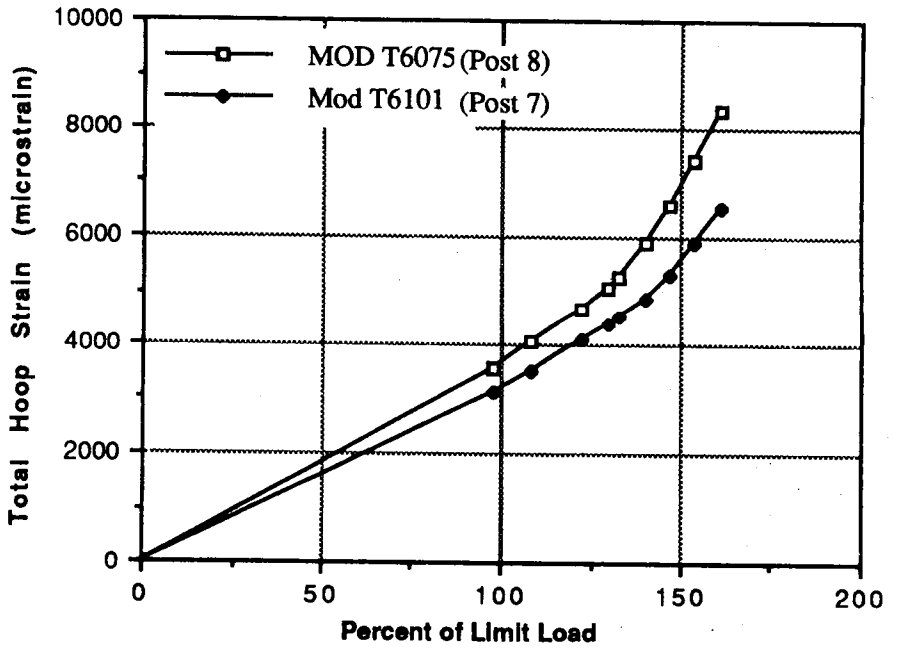

Figure 37. Predicted Strains at T6075 and T6101 (Z = 0.25 in.)

Figures 38 through 41 show the measured strains versus load for post 7 at the same four strain gages compared to the measured post 8 strains at corresponding post 8 gages. The strain gages at post 7 track those at post 8 very closely except for the gages at the aft ring centerline. This is the only location where the measured post 8 strain is significantly greater than the post 7 strain. The post 7 strain lags the post 8 strain as much as 25% at this point. This gage location on post 7 showed strain at post 7 failure equal to the post 8 strain at this location at post 8 failure. This is considered to be the critical gage location. As a result of inspection, the aft ring centerline is believed to be the initial failure point of the STA-2B test and is suspected in the STA-3 test. The detailed nonlinear finite element model shows the highest strains in the weld at this location. Also, it is here that the weld is closest to the post and therefore more susceptible to material variations and/or stresses induced during manufacture.

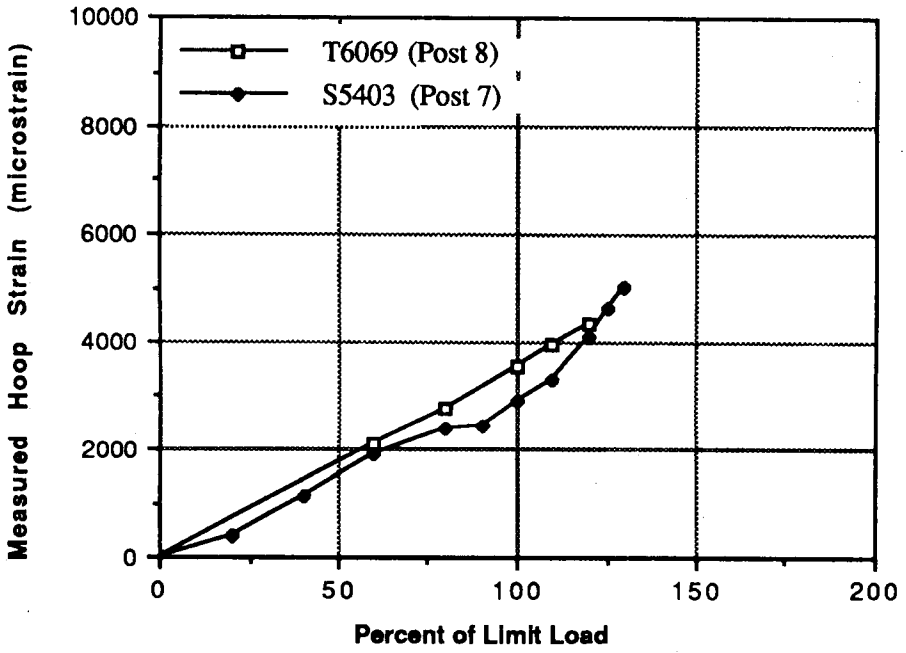

Figure 38. Gages T6069 and S5403 (Z = 7.42 in.)

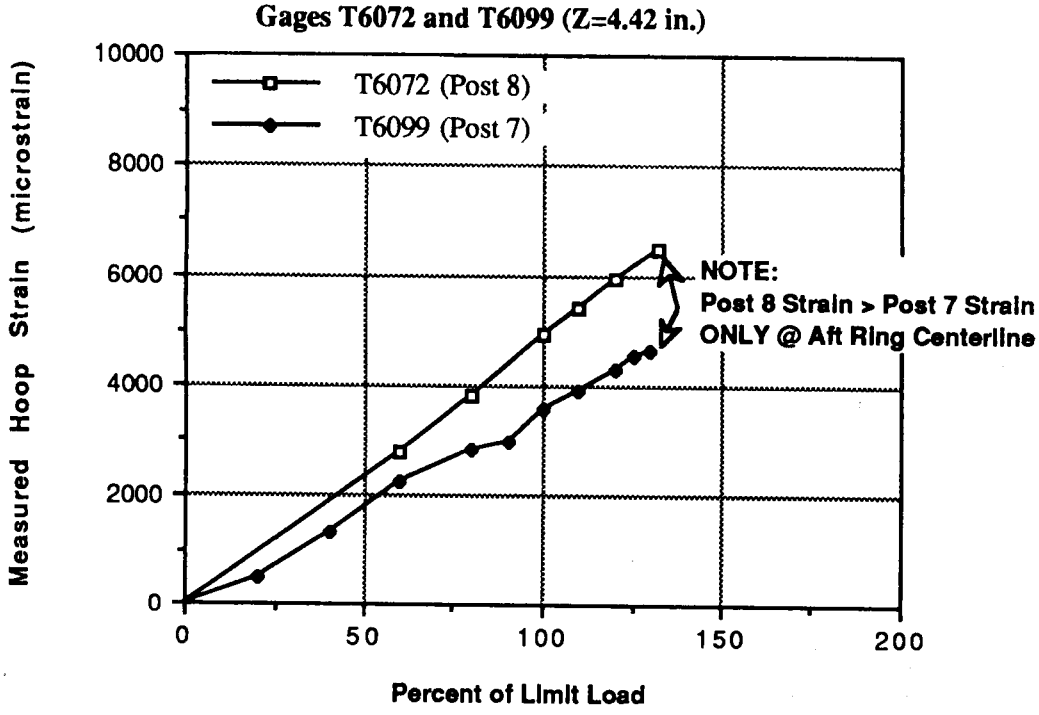

Figure 39. Gages T6072 and T6099 (Z = 4.42 in.)

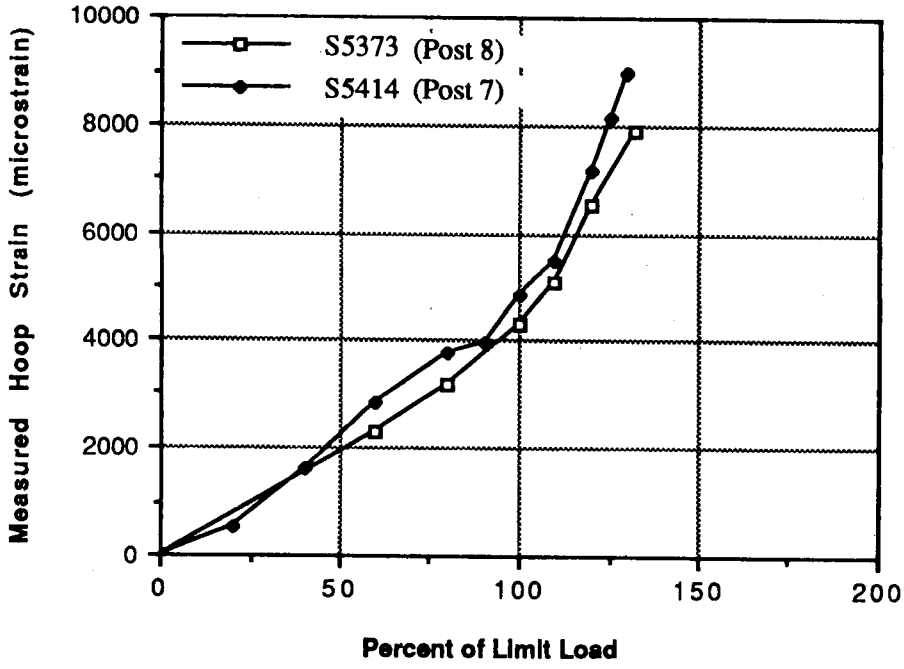

Figure 40. Gages S5373 and S5414 (Z = 2.21 in.)

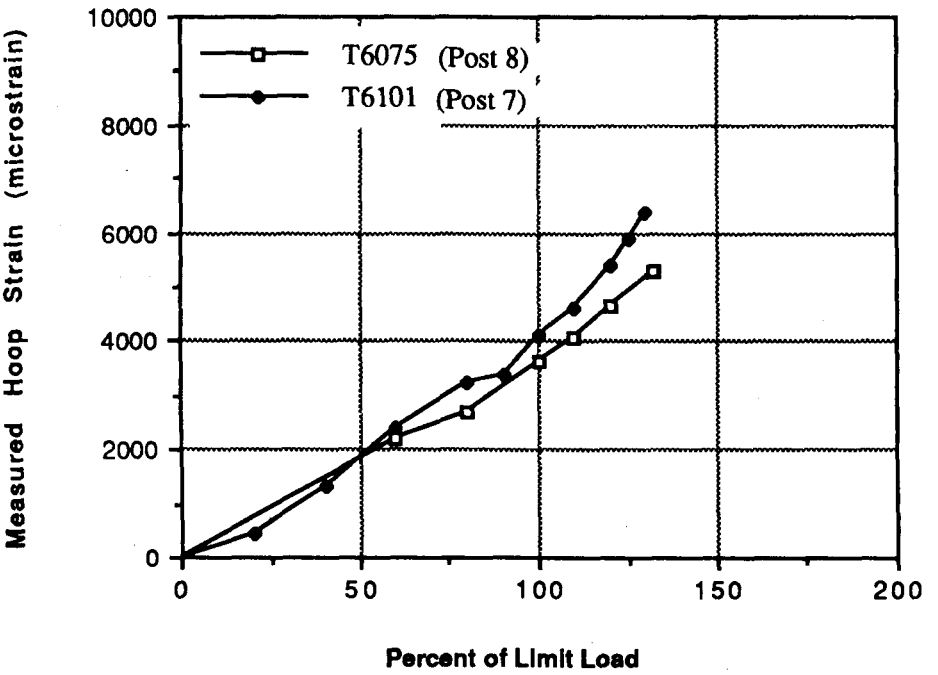

Figure 41. Gages T6075 and T6101 (Z = 0.25 in.)

The finite element analysis is based on nominal dimensions and assumes no pre-stresses due to fabrication. Also, the analysis is sensitive to small material property variations. This sensitivity is shown in Figures 42 through 45 in which the strain predicted at post 8 using both minimum (pretest) and typical (post-test) properties is compared to the actual strain measured by the gages. Results from the analysis and comparison of posts 7 and 8 are as follows:

(1) The gross strain behavior of the posts is essentially the same.

(2) The differences between the two posts are highly localized in the most critical area

(3) The differences between the two posts are not apparent in the analysis.

(4) The analysis is sensitive to material properties and is based on nominal dimensions.

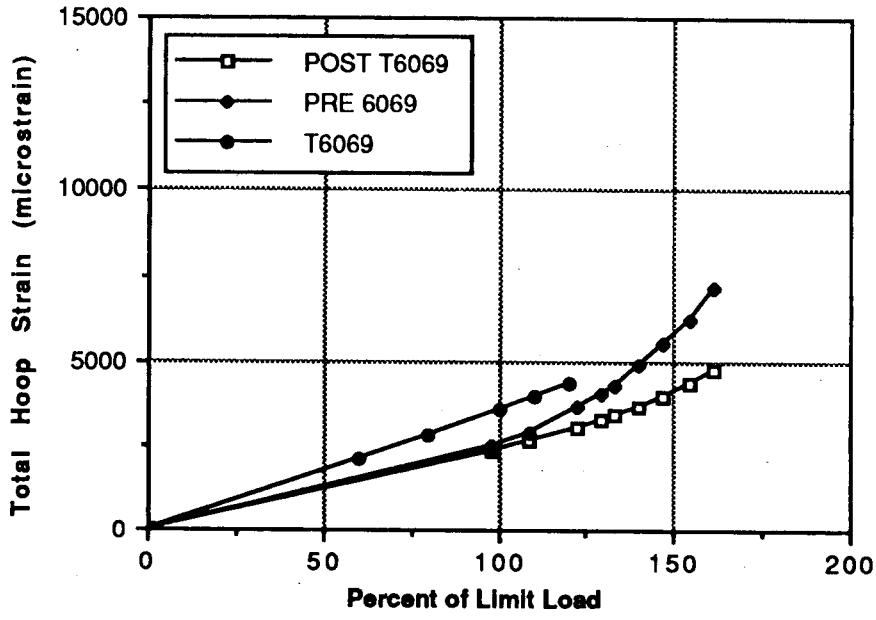

Figure 42. Pretest and Post-Test Analyses versus Actual Strains at Gage T6069

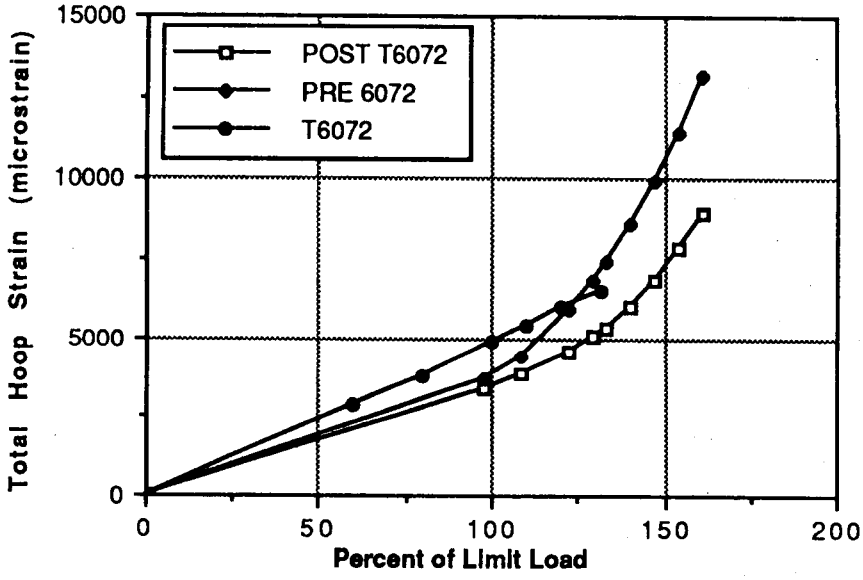

Figure 43. Pretest and Post-Test Analyses versus Actual Strains at Gage T6072

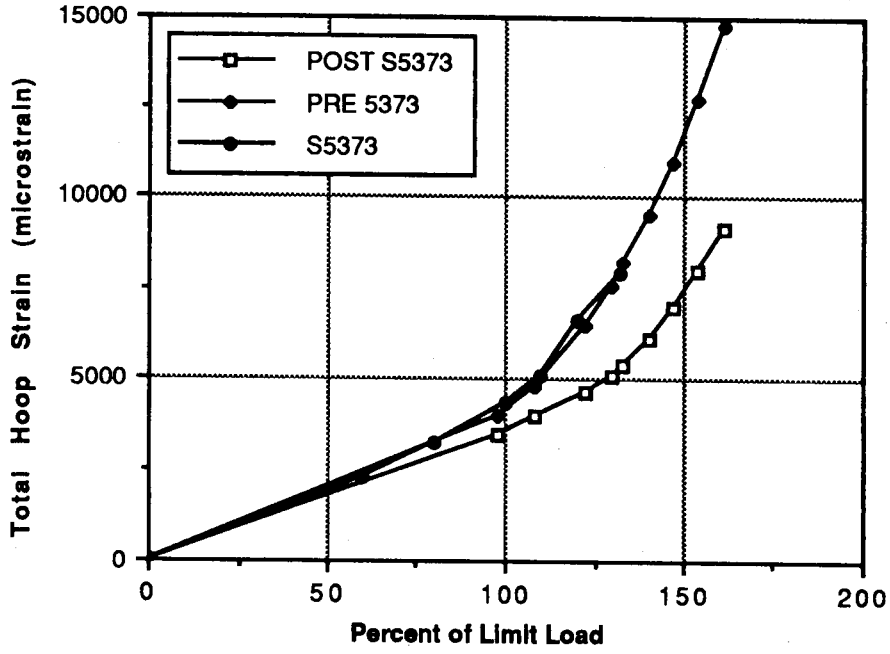

Figure 44. Pretest and Post-Test Analyses versus Actual Strains at Gage S5373

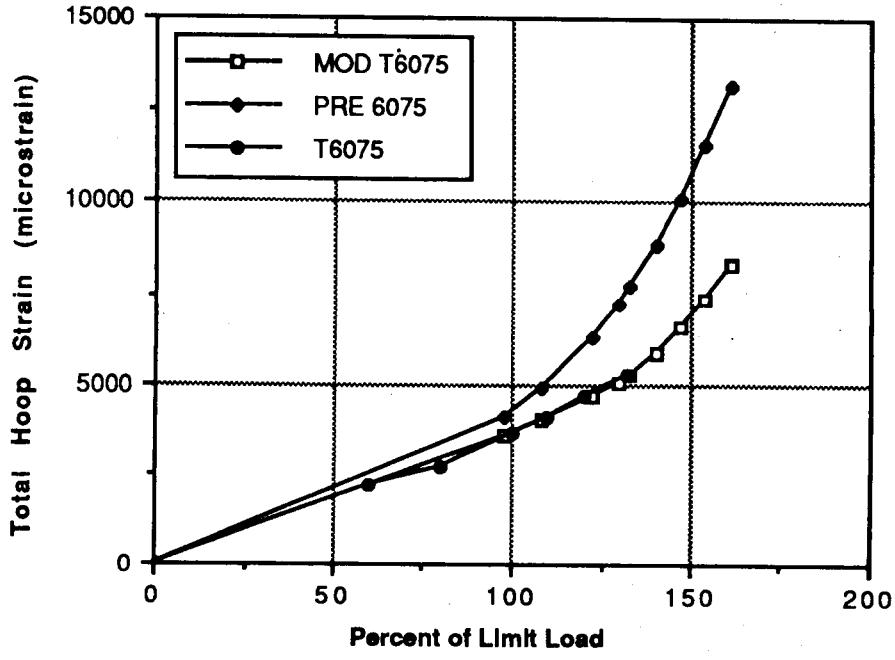

Figure 45. Pretest and Post-Test Analyses versus Actual Strains at Gage T6075

From the above results the following conclusions are drawn:

(1) The apparent difference in strength between the posts is probably due to small and non-repeatable manufacturing variables and load redistribution.

(2) The apparent greater strength of post 7 is not repeatable.

(3) The reliable strength of both posts is the same.

6. DISCUSSION OF RESULTS

6.1 MODEL VALIDITY

The finite element analysis has been shown to be accurate through multiple comparisons to test data. This is true for both the original design and the redesign in both linear and nonlinear analyses. These were discussed previously and are summarized below.

1) Stresses predicted by the detailed finite element model matched the Wyle influence test strain gage data in the area of the post to skin fillet within an average of 6% for radial and axial loads on the original design.
(2) The nonlinear strains predicted by the detailed model match the strain gages in the failure area of the STA-3 test very well, though two of the gages are slightly under predicted.
(3) The pretest analysis predicted a 50% reduction in strain from STA-2B loads to STA-3 loads. The gage located on the aft ring centerline during the STA-3 test consistently measured strains 40% below a similarly located gage during STA-2B.
(4) Test specimens were modeled using methods similar to those used to model the aft skirt. The results, while under-predicting the strain levels, were in reasonable agreement with tension tests of the specimens.

6.2 ANALYSIS RESULTS

The critical area where failure most likely initiated is the forging HAZ at the aft ring centerline (approximately 4.4 in. from the bottom of the post). The largest total hoop strain *in the HAZ* occurs at this location. This is true even though the gage located at the aft ring centerline does not show strains as high as the gages immediately above it. This was shown previously in Figures 20 and 23 using minimum and typical material properties, respectively. This was also seen in the strain contours in Figures 12, 13, 24, and 25. It is in this area that the weld is closest to the post.

The stress/strain state near the failure area is sensitive to material property changes. This sensitivity is increased in the nonlinear range. The difference between using minimum as opposed to using typical properties was greater than 0.5% strain. Different combinations

of properties (for example, typical forging and minimum weld properties) can also affect the stress level, but this effect seems to be slight.

The finite element model shows no significant difference between the strain levels of post 8 and post 7. Of the four gages in the failure area, three gages show no significant difference between posts 7 and 8. However, the gage at the aft ring centerline shows the strain in post 8 to be 25% higher than the strain at the same location in post 7. Although the gross behavior of posts 7 and 8 is the same, there is a highly localized difference in the strain state of posts 7 and 8 that is not apparent in the analysis.

The geometry of this location also contributes to a possible failure scenario in the following ways.

(1) The weld meets the edge of a fillet on both the inner and outer surfaces of the skin at this location. This causes stress concentrations and other effects due to the thick post meeting the thin skin.

(2) The proximity of the weld to the large mass of the post makes this location a likely spot for any heating or cooling related material anomalies caused during manufacture.

(3) The HAZ is thinnest at this spot due to more rapid cooling during welding.

7. CONCLUSIONS

The analysis has confirmed the area of failure in both STA-2B and STA-3 tests as being the forging HAZ at the aft ring centerline. The highest hoop strain in the HAZ occurs in this area. The analysis results correlate well with strain gage data from both the Wyle influence test of the original design Aft Skirt and the STA-3 test of the redesigned Aft Skirt. However, the analysis *does not* predict failure as defined by ultimate elongation of the material equal to 3.5% total strain.

The STA-3 test results point to a highly localized area being the origin of the failure. This area is the weld zone close to the aft ring centerline. Post 8 strain gage readings are significantly higher than post 7 strain gage readings only in this area. The measured strains *at failure* in this area are the same for both post 7 and post 8.

All the analytical findings in this study point to the same area and define it more narrowly as the forging HAZ at the aft ring centerline. The analysis clearly shows the highest strain in the HAZ occuring in this area and correlates with all the strain gages in the Post 8 failure area. This indicates that the stress/strain state of the failure region, while being complex, is understood and modeled accurately.

The analytical model of post 7 does not show the large difference in strains at the aft ring centerline that the STA-3 data show. This indicates a highly localized difference in the strain states of posts 7 and 8 that is due to a variation not accounted for in the analytical model.

The Aft Skirt material has been shown to be sensitive to manufacturing variables such as weld schedule. The geometry of the failure region also contributes to added sensitivity to manufacturing or processing variables in the following ways:

(1) The weld meets the edge of a fillet on both the inner and outer surfaces of the skin at this location. This causes stress concentrations and other effects due to the thick post meeting the thin skin.

(2) The proximity of the weld to the large mass of the post makes this location a likely spot for any heating or cooling related material anomalies caused during manufacture.

(3) The HAZ is thinnest at this spot due to more rapid cooling during welding. At this time there are few data concerning the material properties and strengths in this particular local region (between 3 and 6 in. from the bottom of the post in the weld area).

We suggest that the sensitivity of the failure area material strength and stress/strain state to material properties and therefore to small manufacturing or processing variables is the most likely cause of failure below the expected material ultimate properties.

Appendix A

INDIVIDUAL SUBSTRUCTURE PLOTS

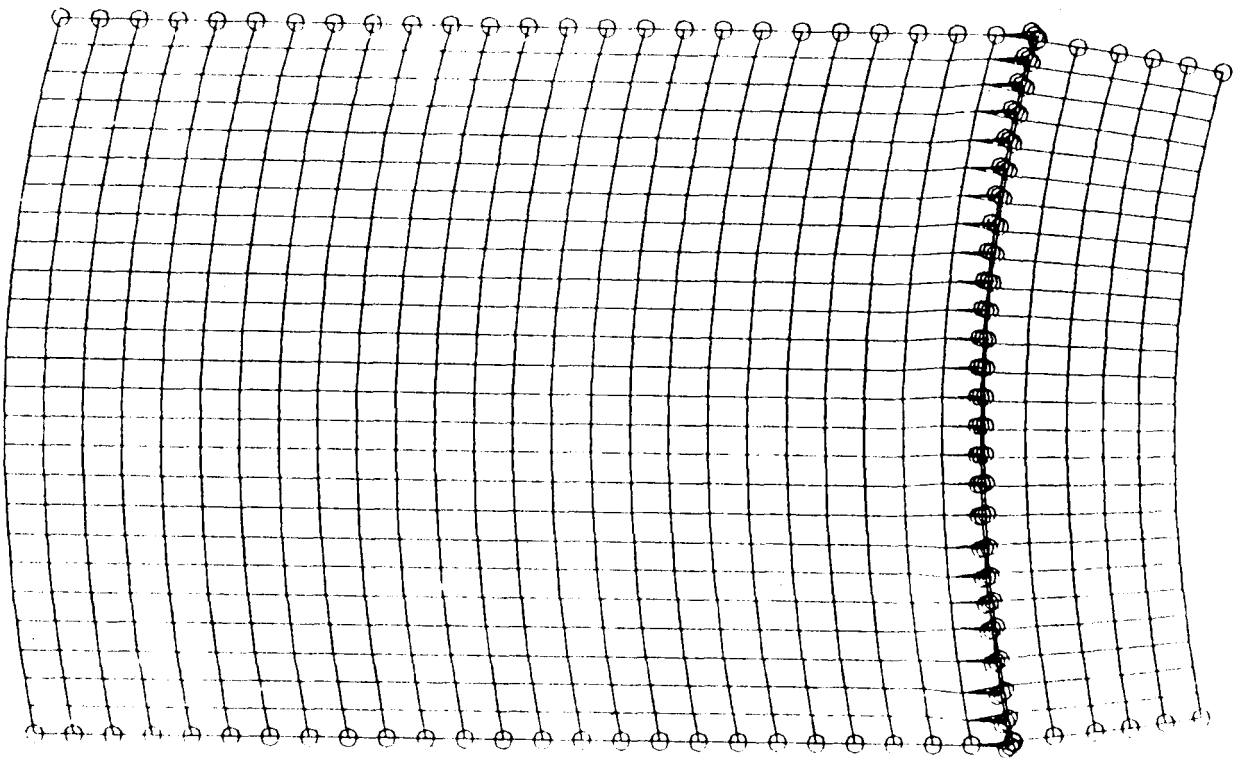

Fig. A-1 Substructure MC1
(Substructure Boundary Nodes Circled)

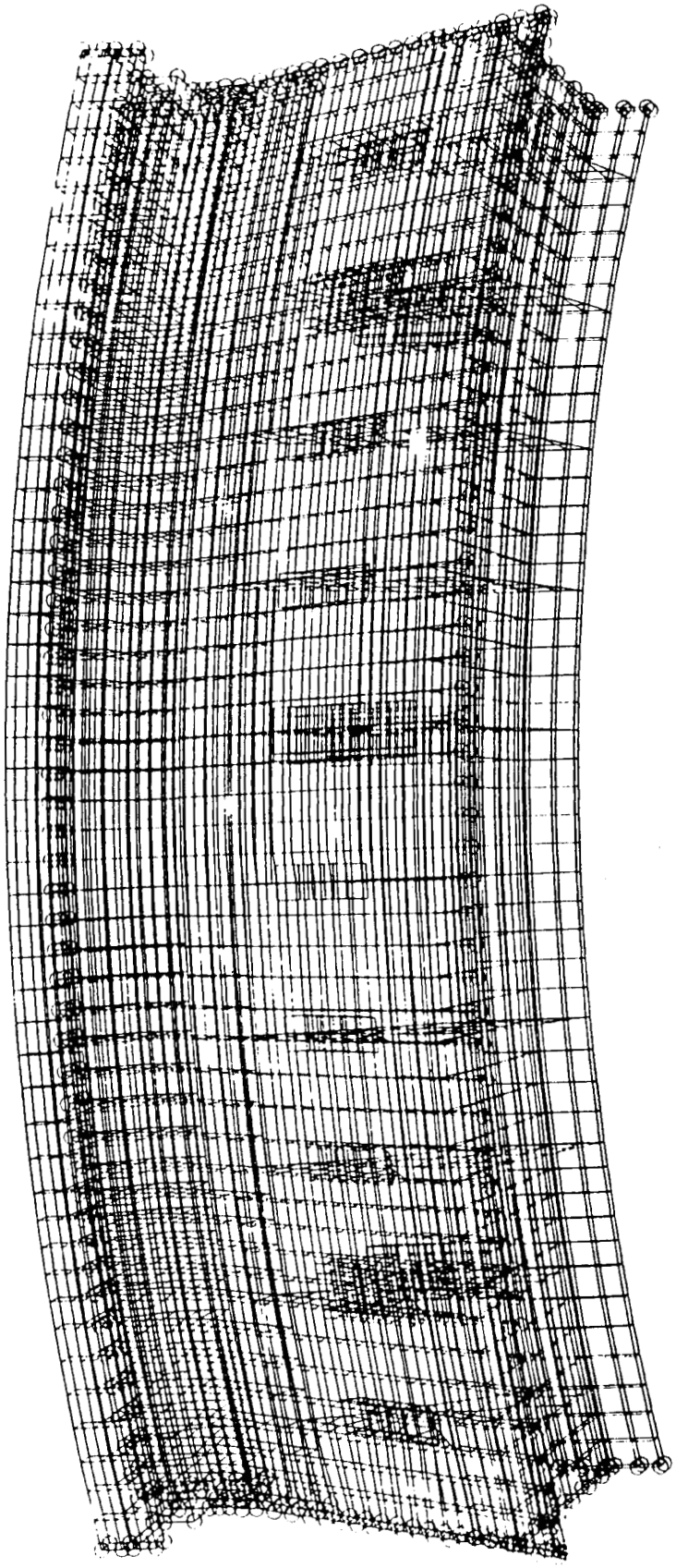

Fig. A-2 Substructure 1A - URG1 - TRG1
(Substructure Boundary Nodes Circled)

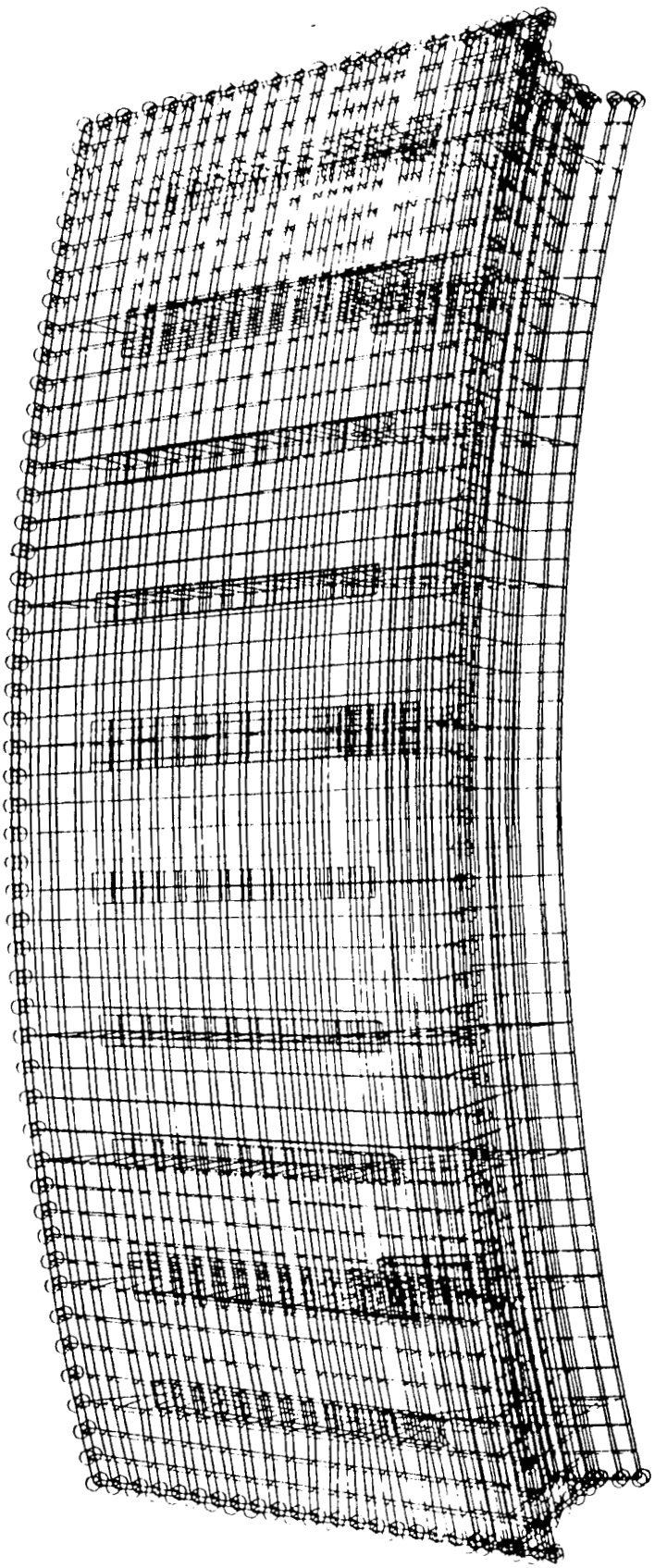

Fig. A-3 Substructure 1B - MRG1
(Substructure Boundary Nodes Circled)

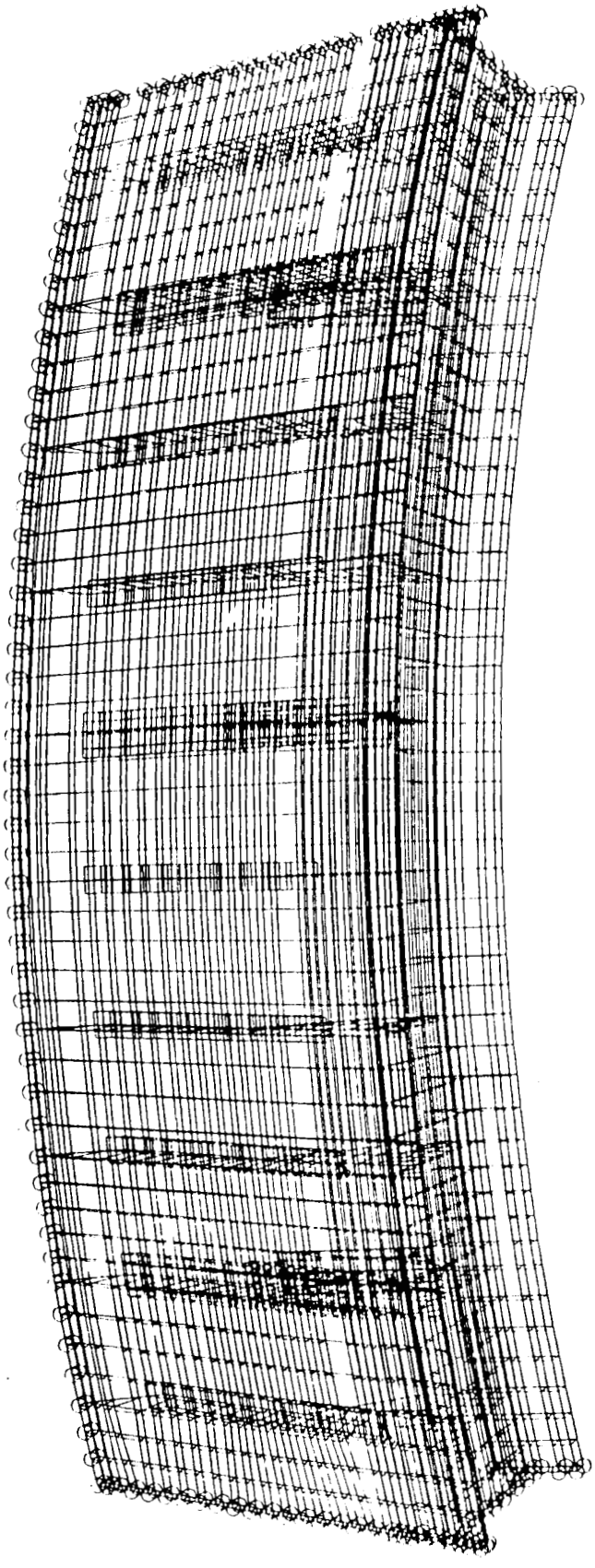

Fig. A-4 Substructure 1C - LRG1
(Substructure Boundary Nodes Circled)

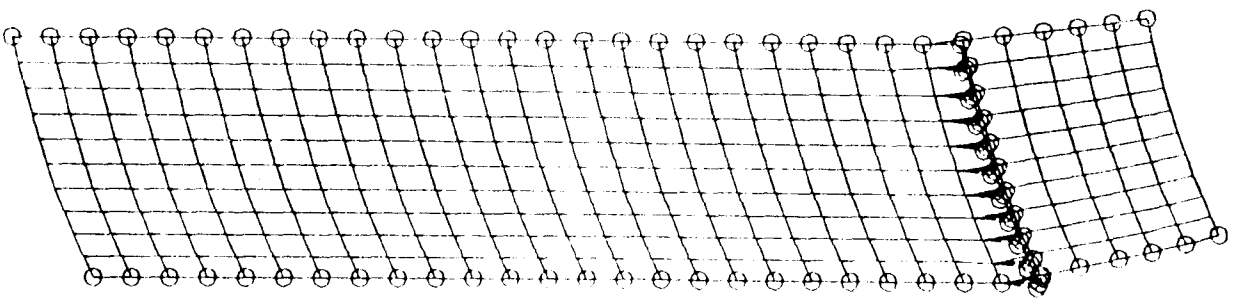

Fig. A-5 Substructure MC2
(Substructure Boundary Nodes Circled)

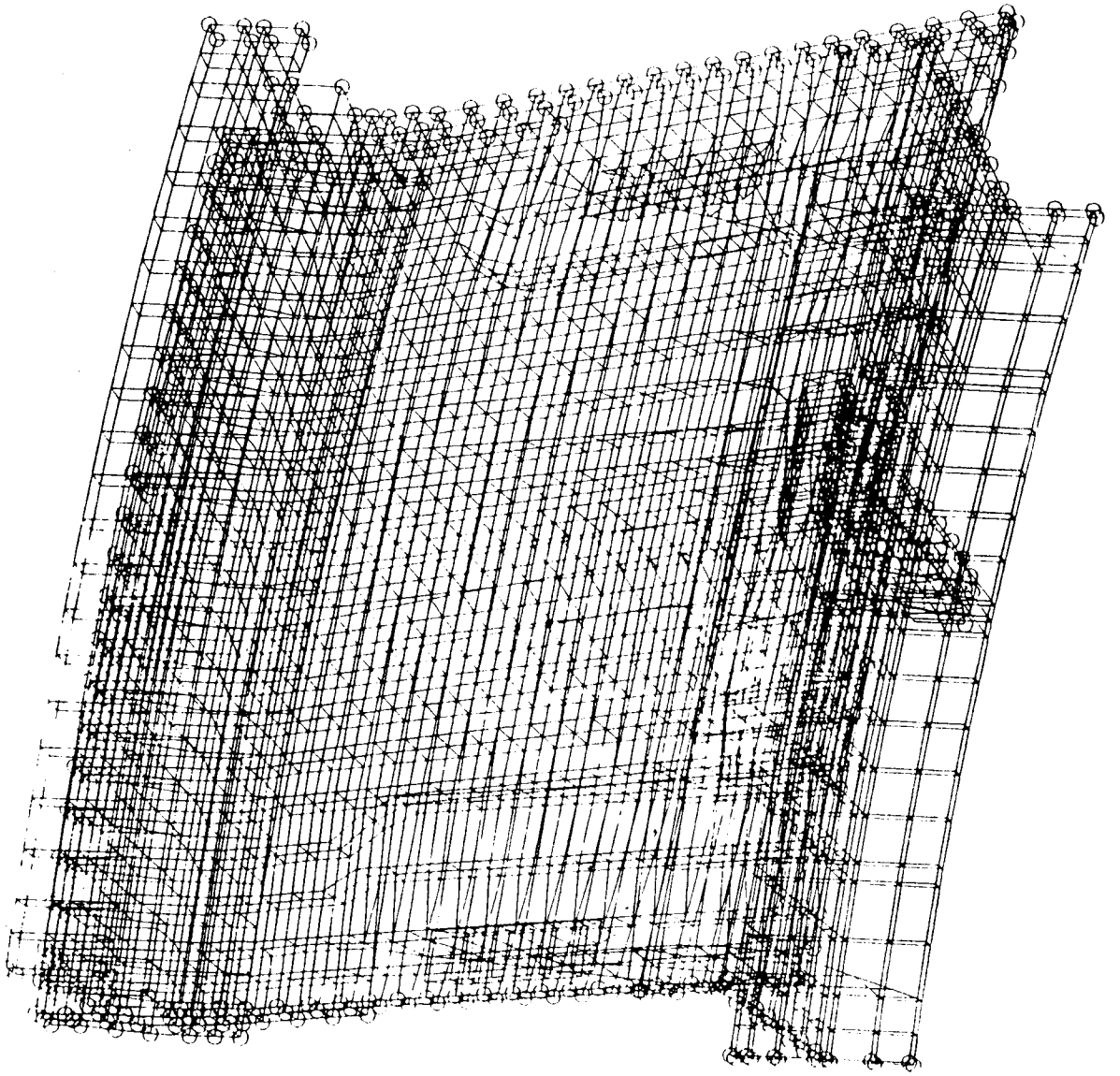

Fig. A-6 Substructure P601
(Substructure Boundary Nodes Circled)

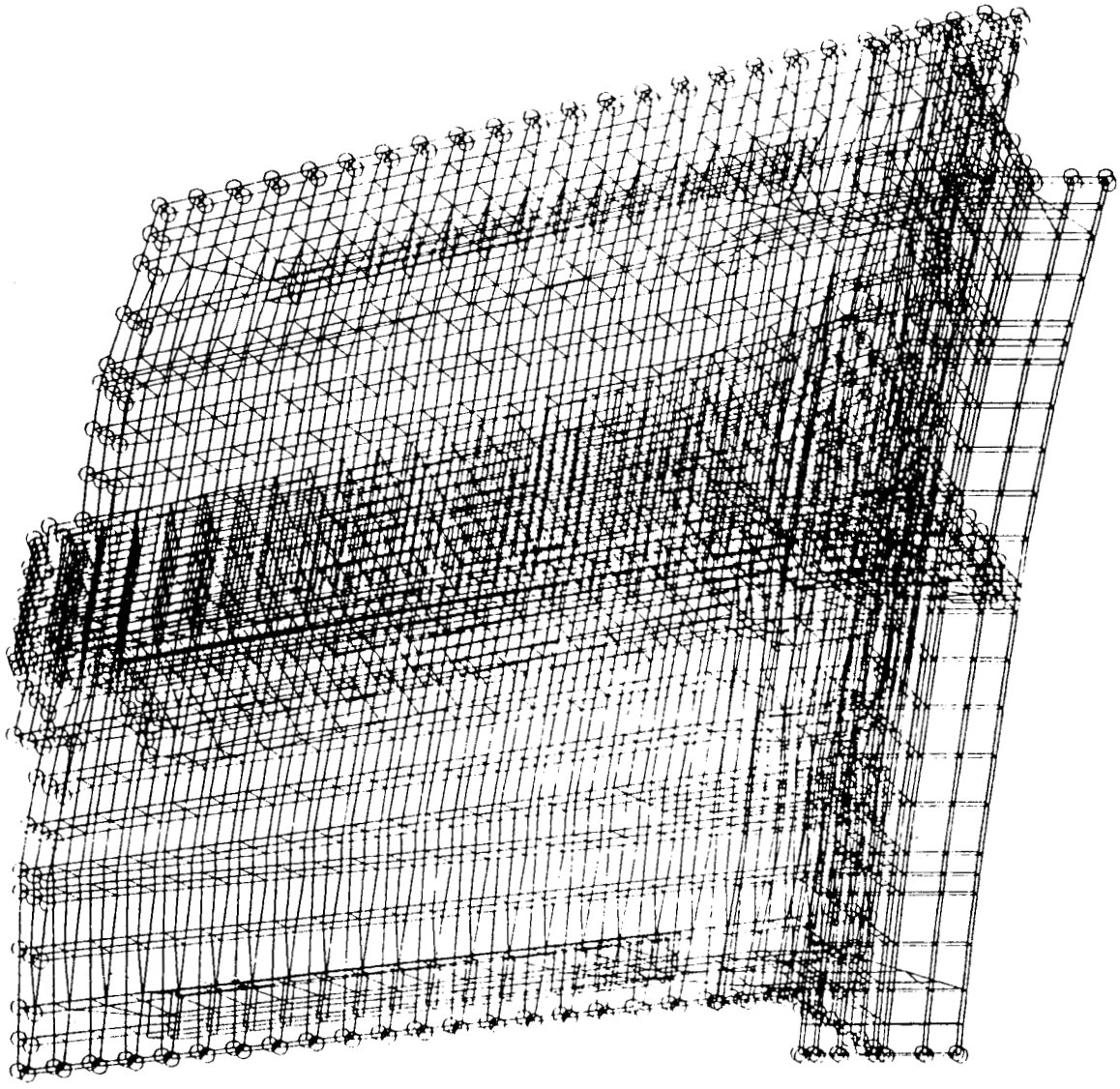

Fig. A-7 Substructure P602
(Substructure Boundary Nodes Circled)

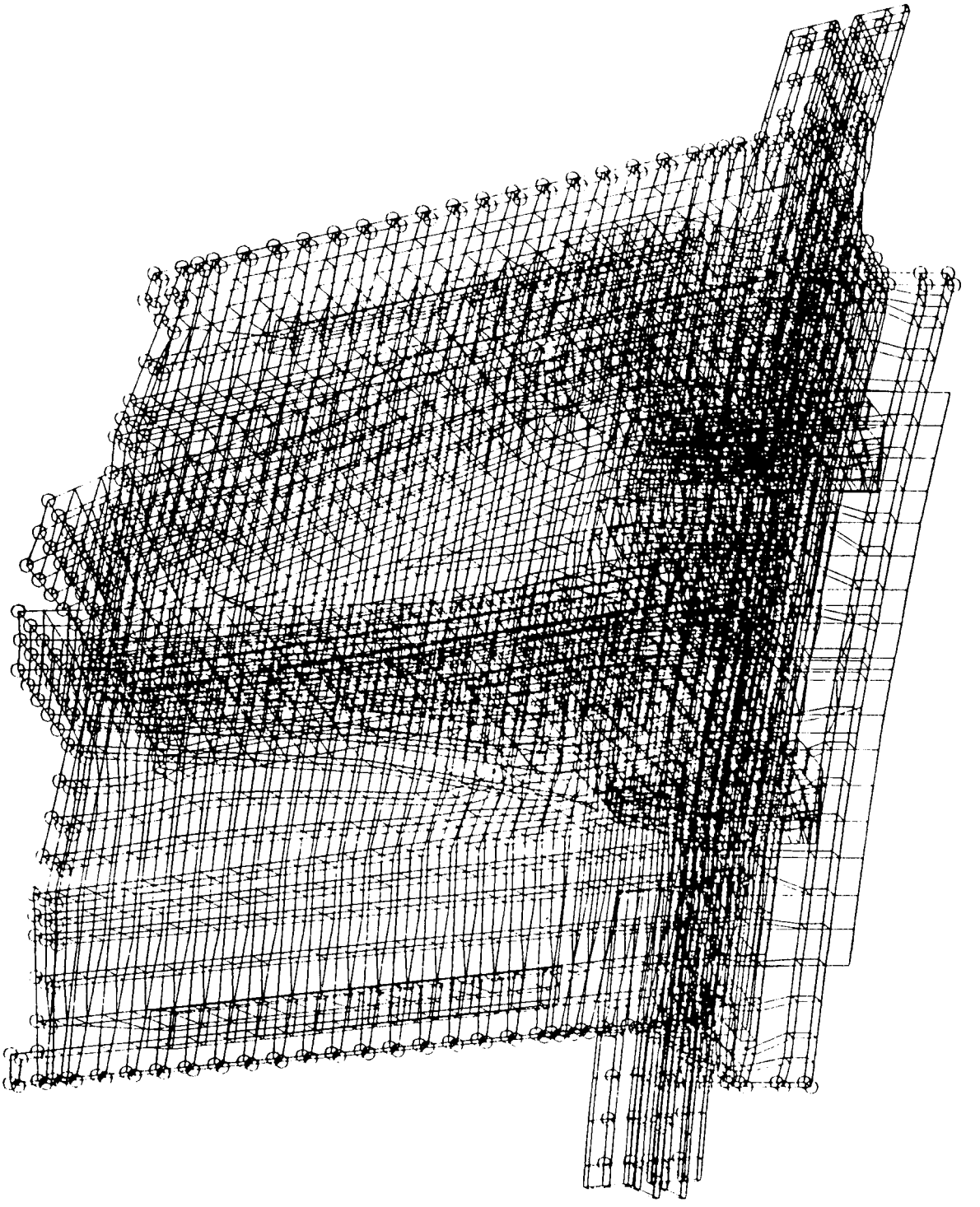

Fig. A-8 Substructure P603
(Substructure Boundary Nodes Circled)

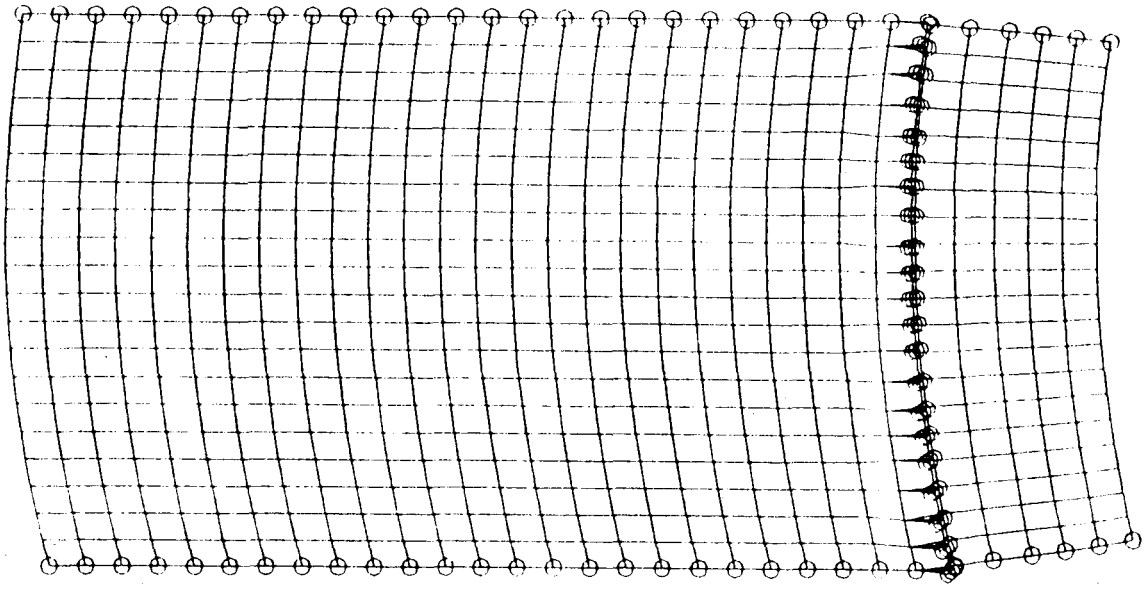

Fig. A-9 Substructure MC3
(Substructure Boundary Nodes Circled)

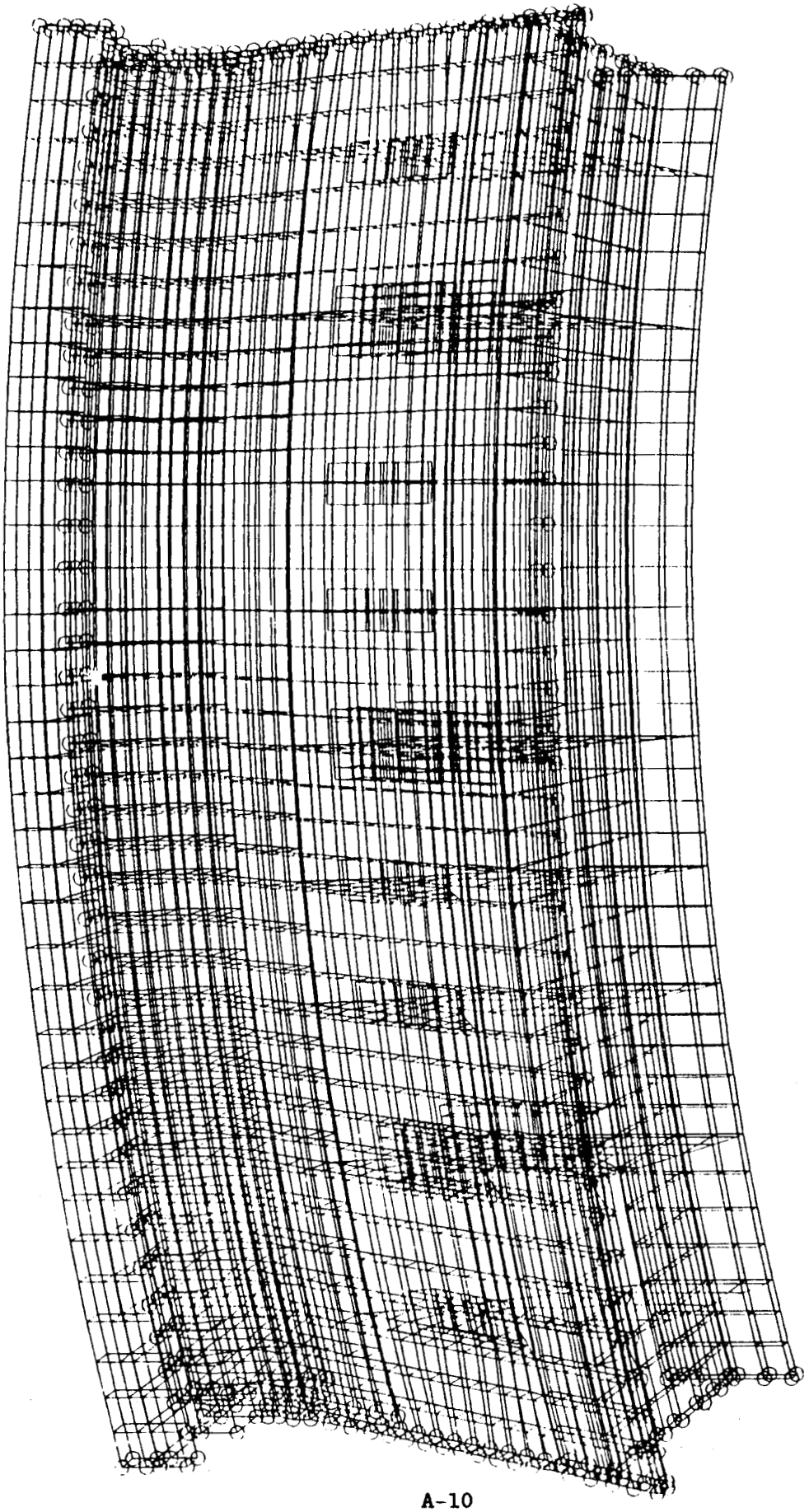

Fig. A-10 Substructure MC3
(Substructure Boundary Nodes Circled)

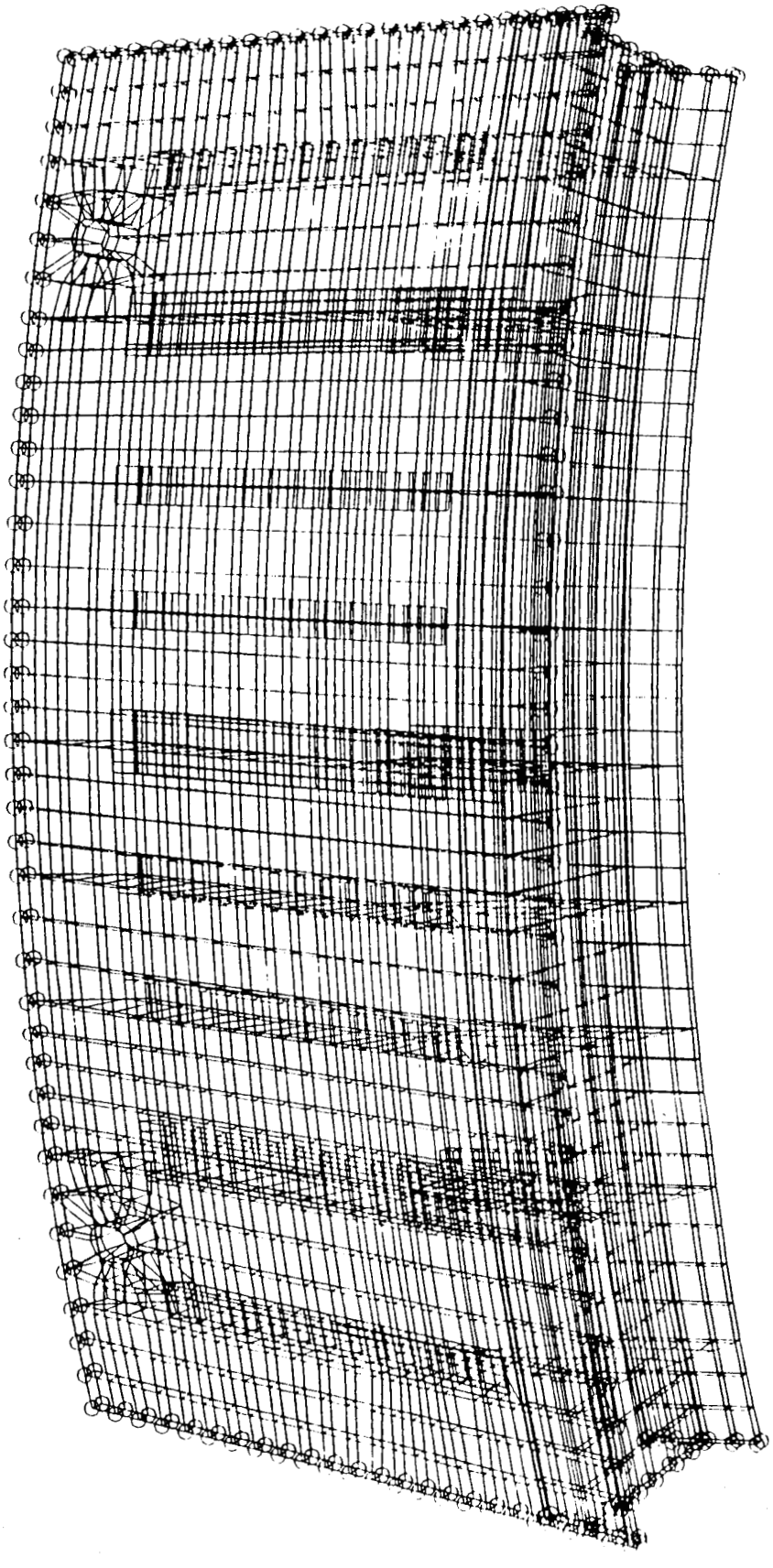

Fig. A-11 Substructure 2B - MRG2
(Substructure Boundary Nodes Circled)

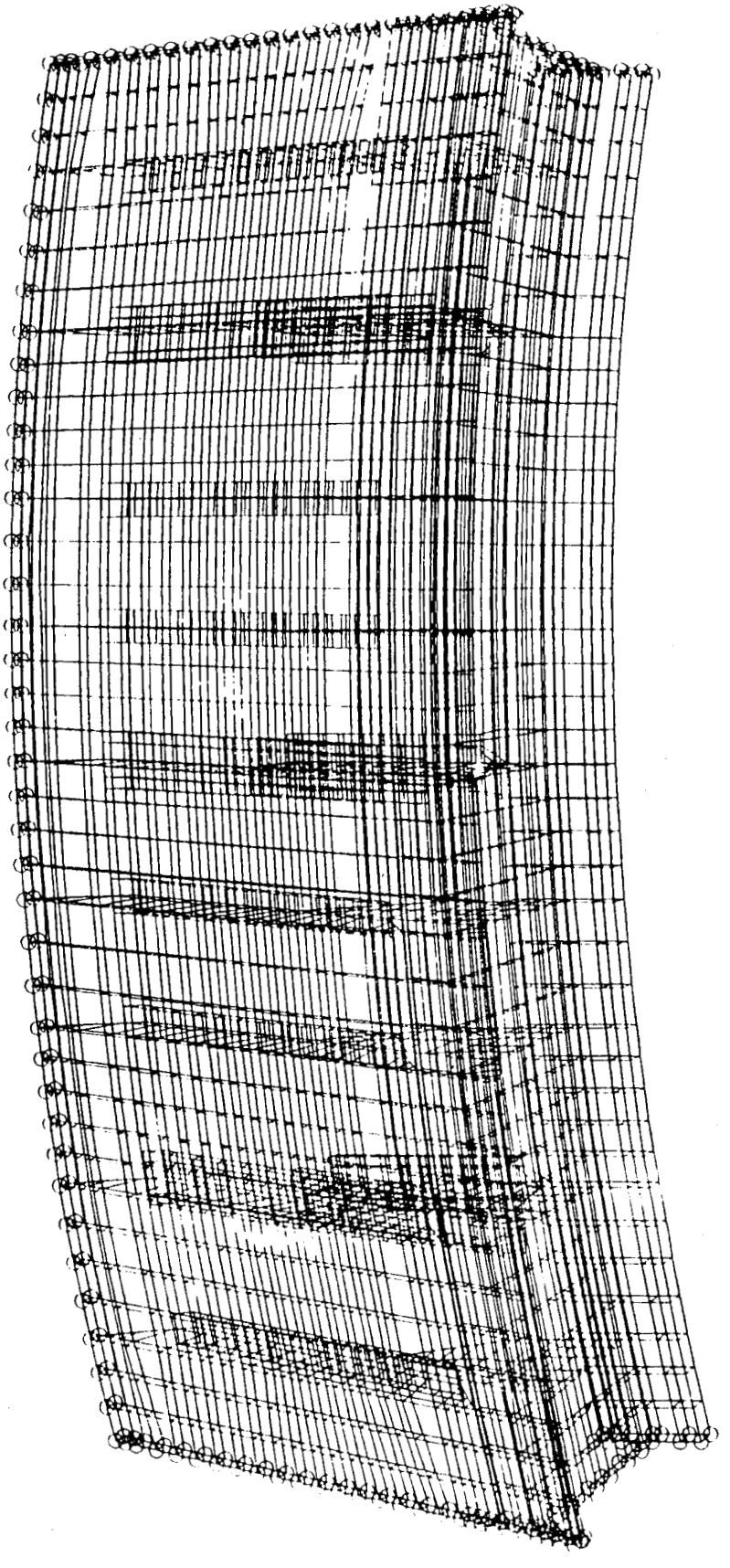

Fig. A-12 Substructure 2C - LRG2
(Substructure Boundary Nodes Circled)

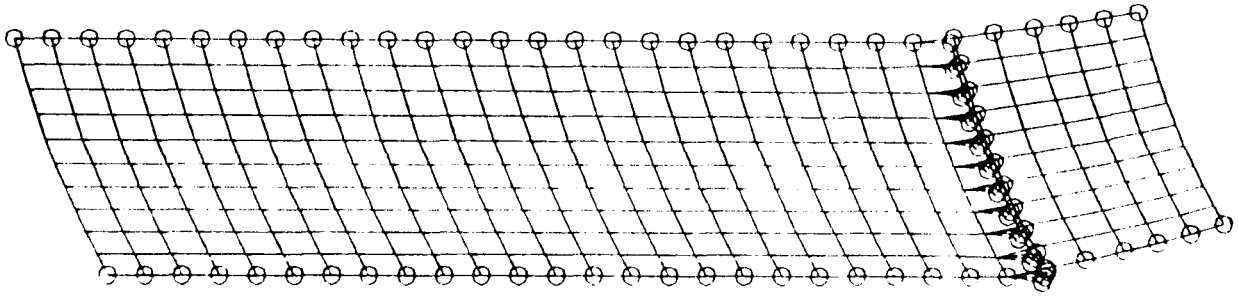

Fig. A-13 Substructure MC4
(Substructure Boundary Nodes Circled)

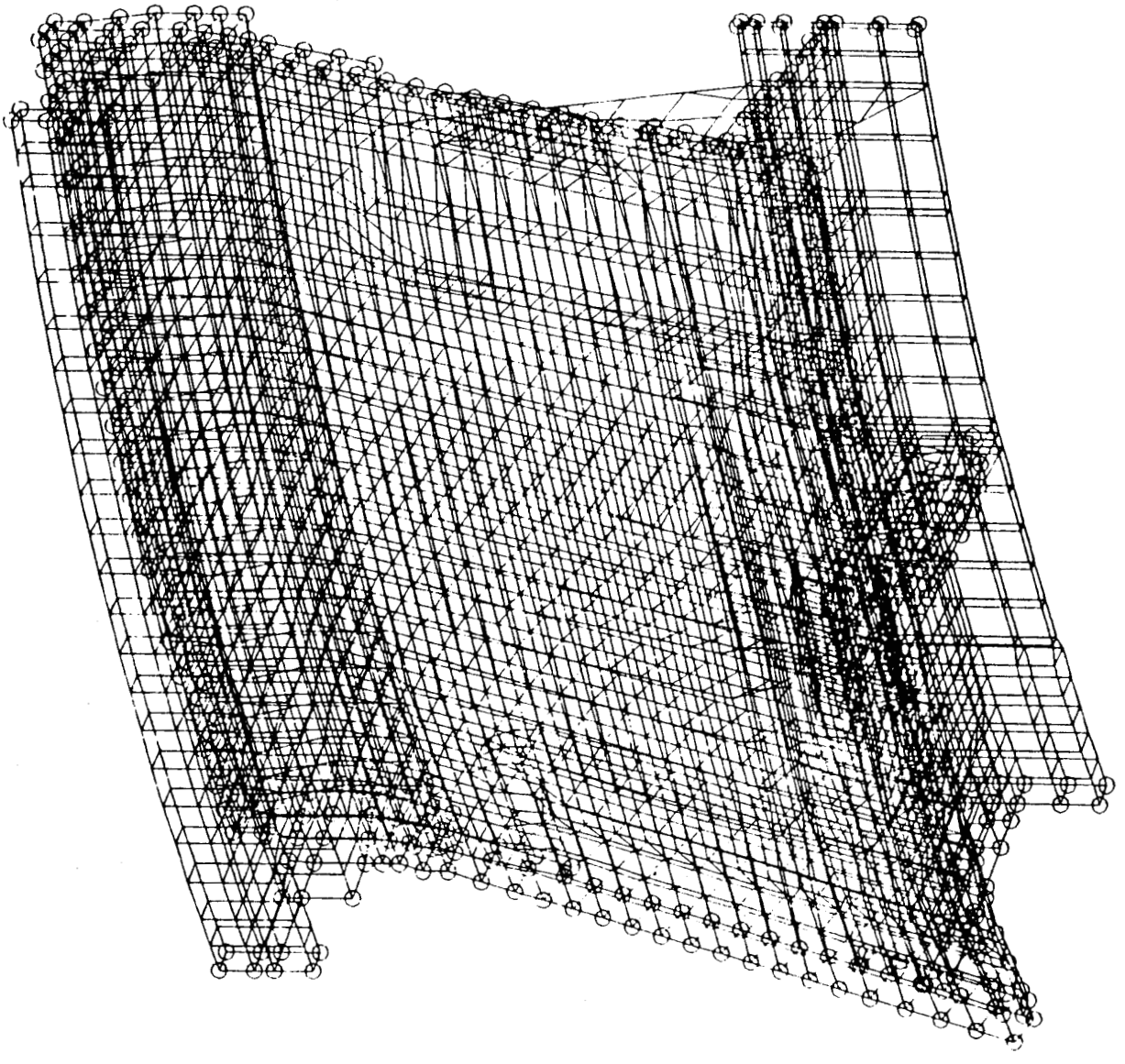

Fig. A-14 Substructure P1201
(Substructure Boundary Nodes Circled)

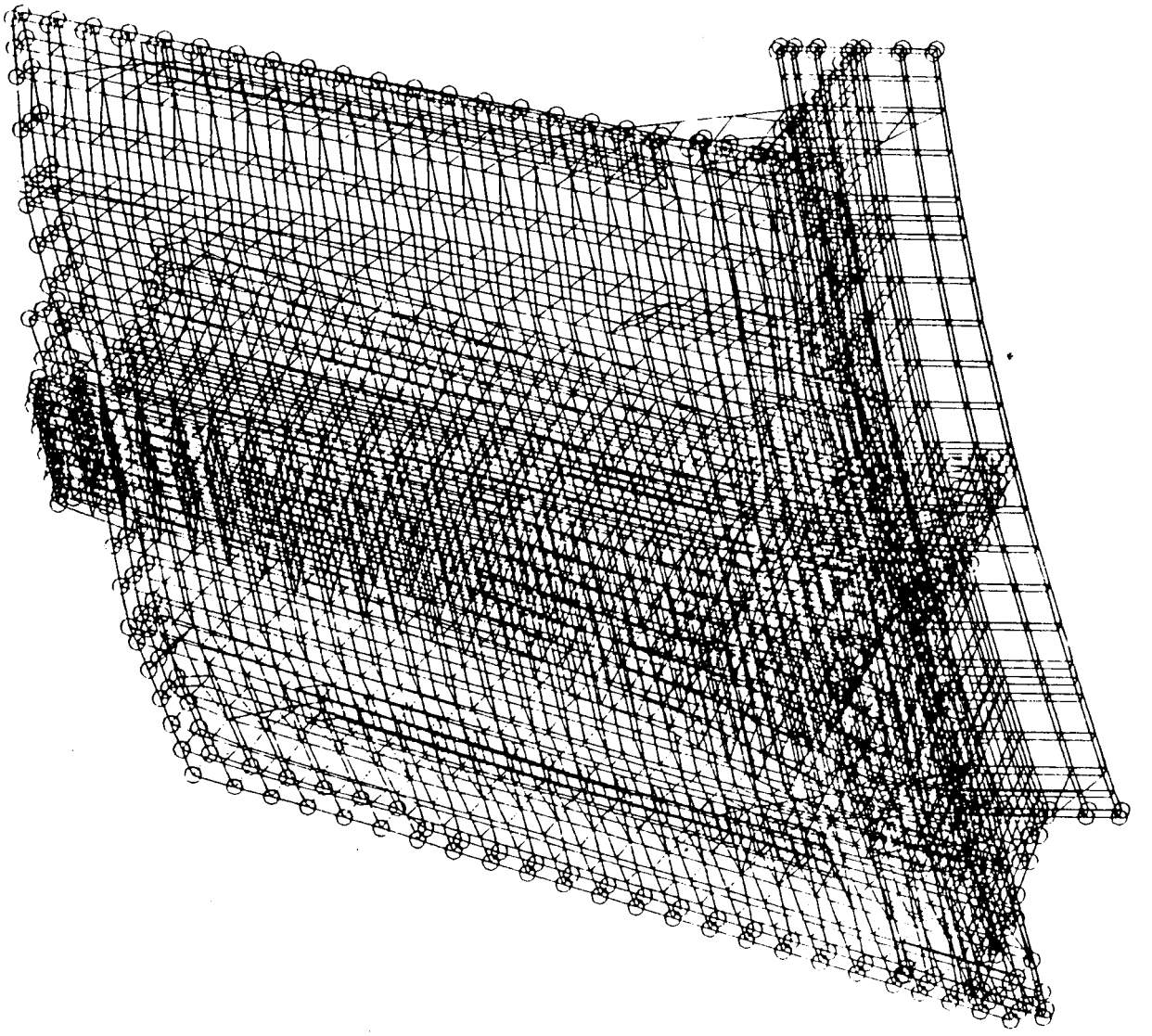

Fig. A-15 Substructure P1202
(Substructure Boundary Nodes Circled)

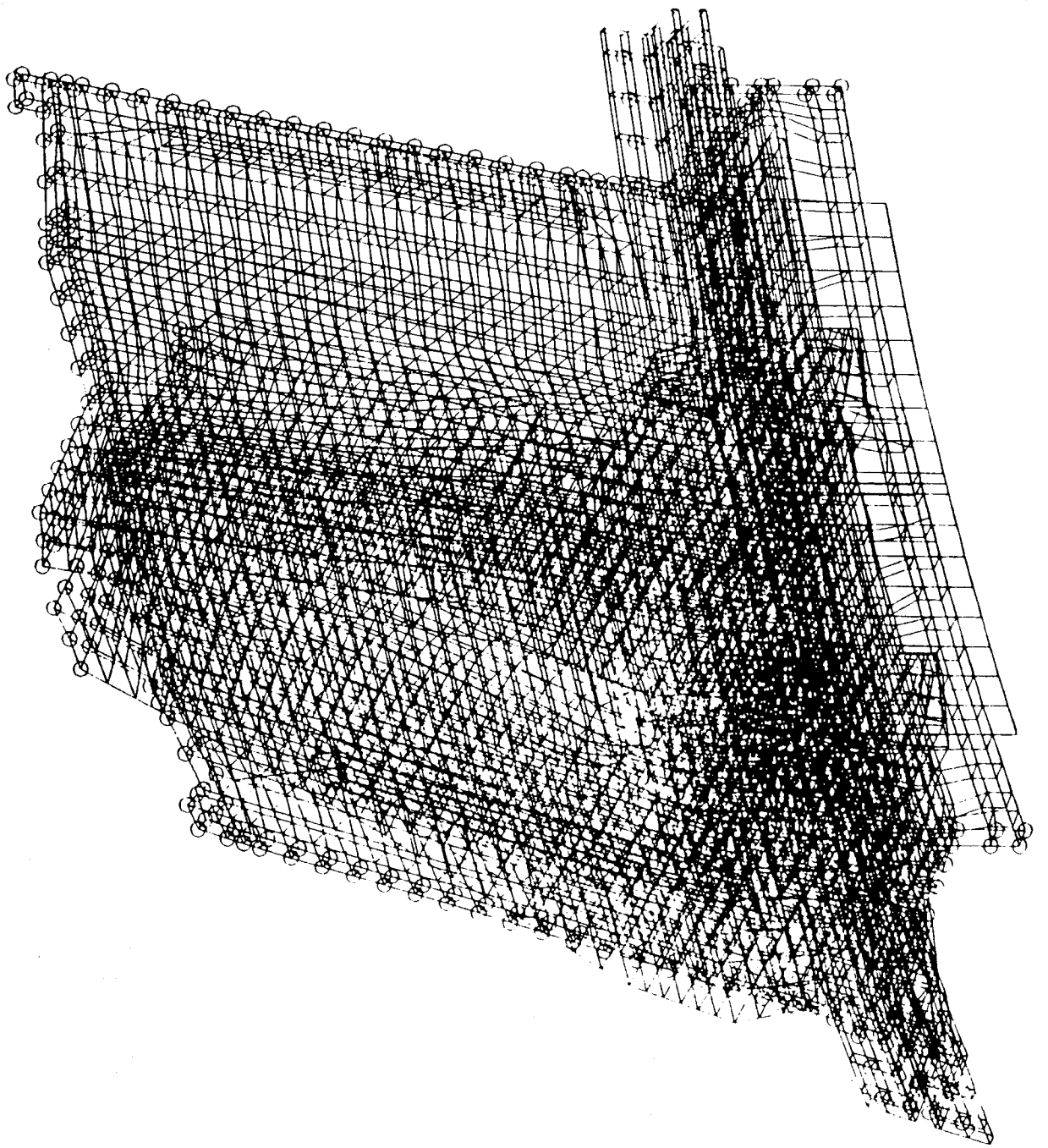

Fig. A-16 Substructure P1203
(Substructure Boundary Nodes Circled)

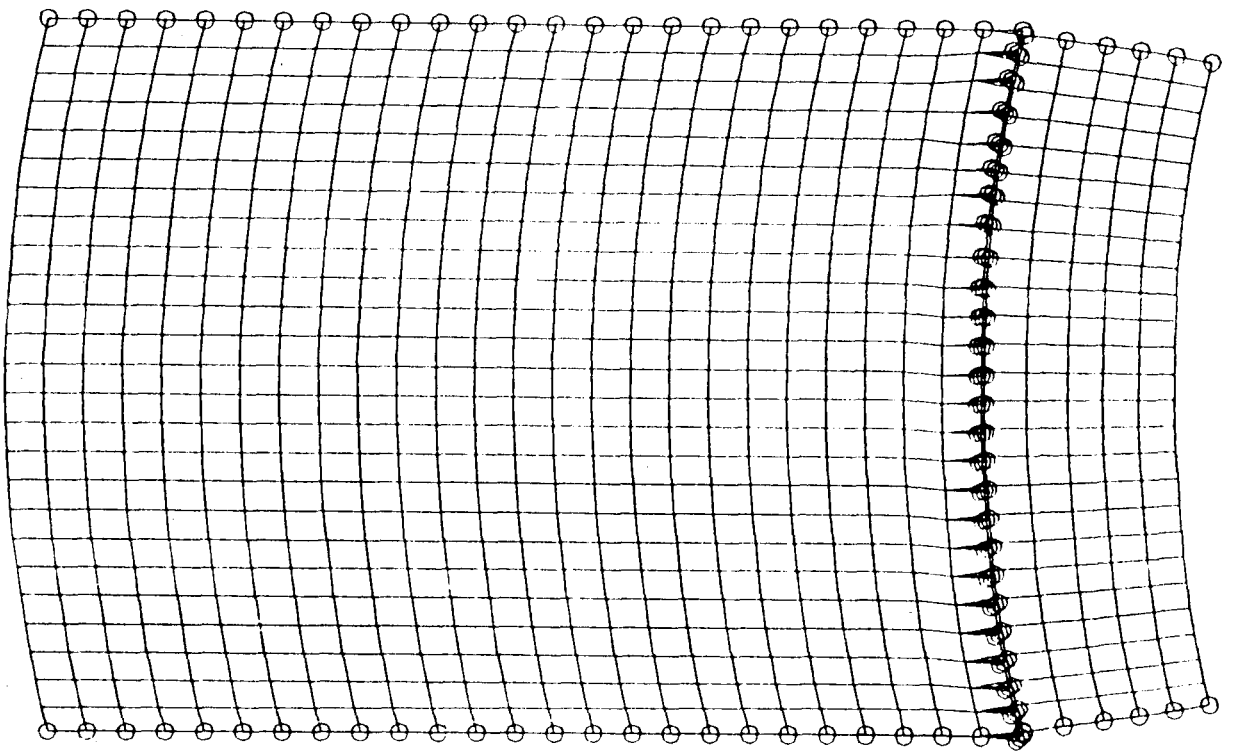

Fig. A-17 Substructure MC5
(Substructure Boundary Nodes Circled)

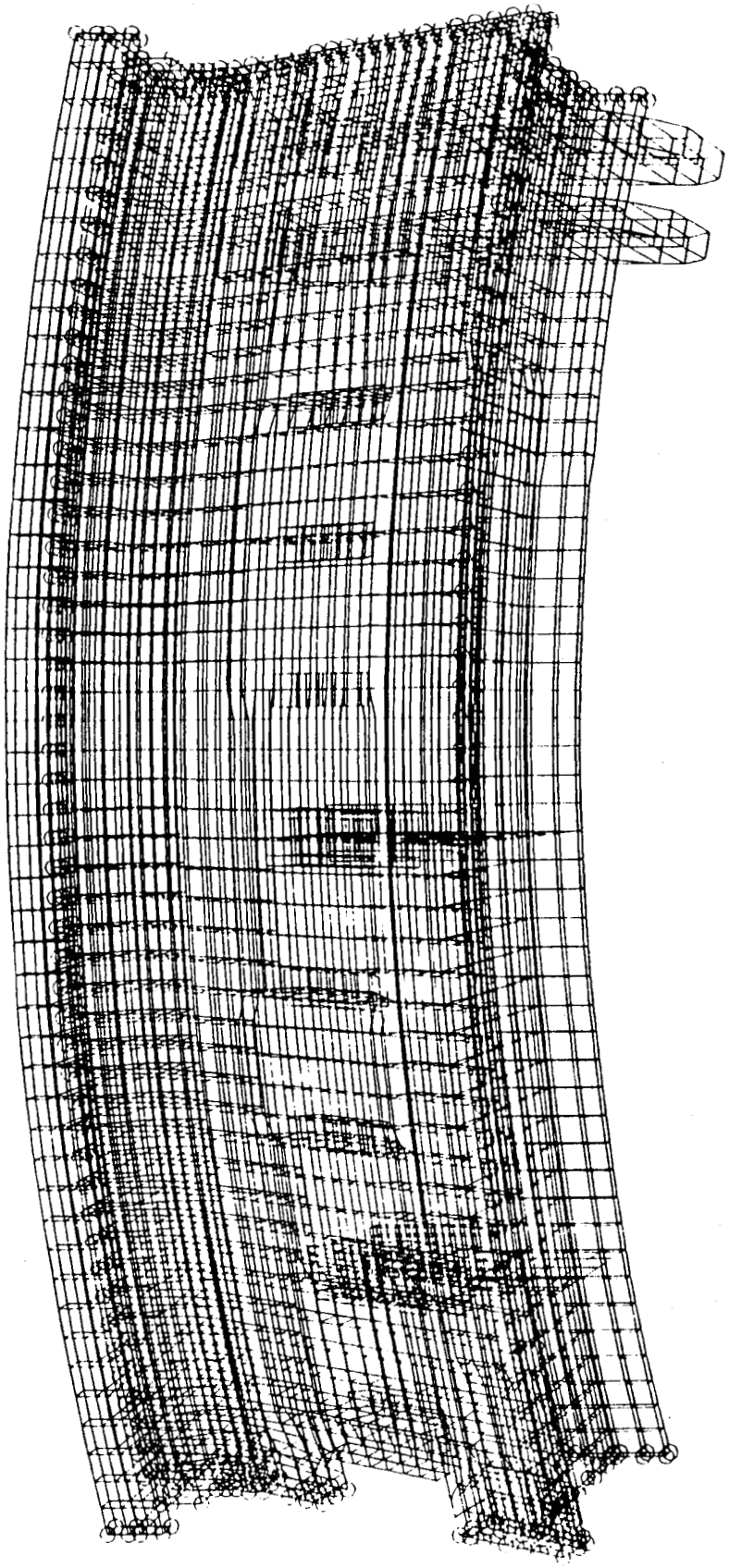

Fig. A-18 Substructure 3A - URG3 - TRG5
(Substructure Boundary Nodes Circled)

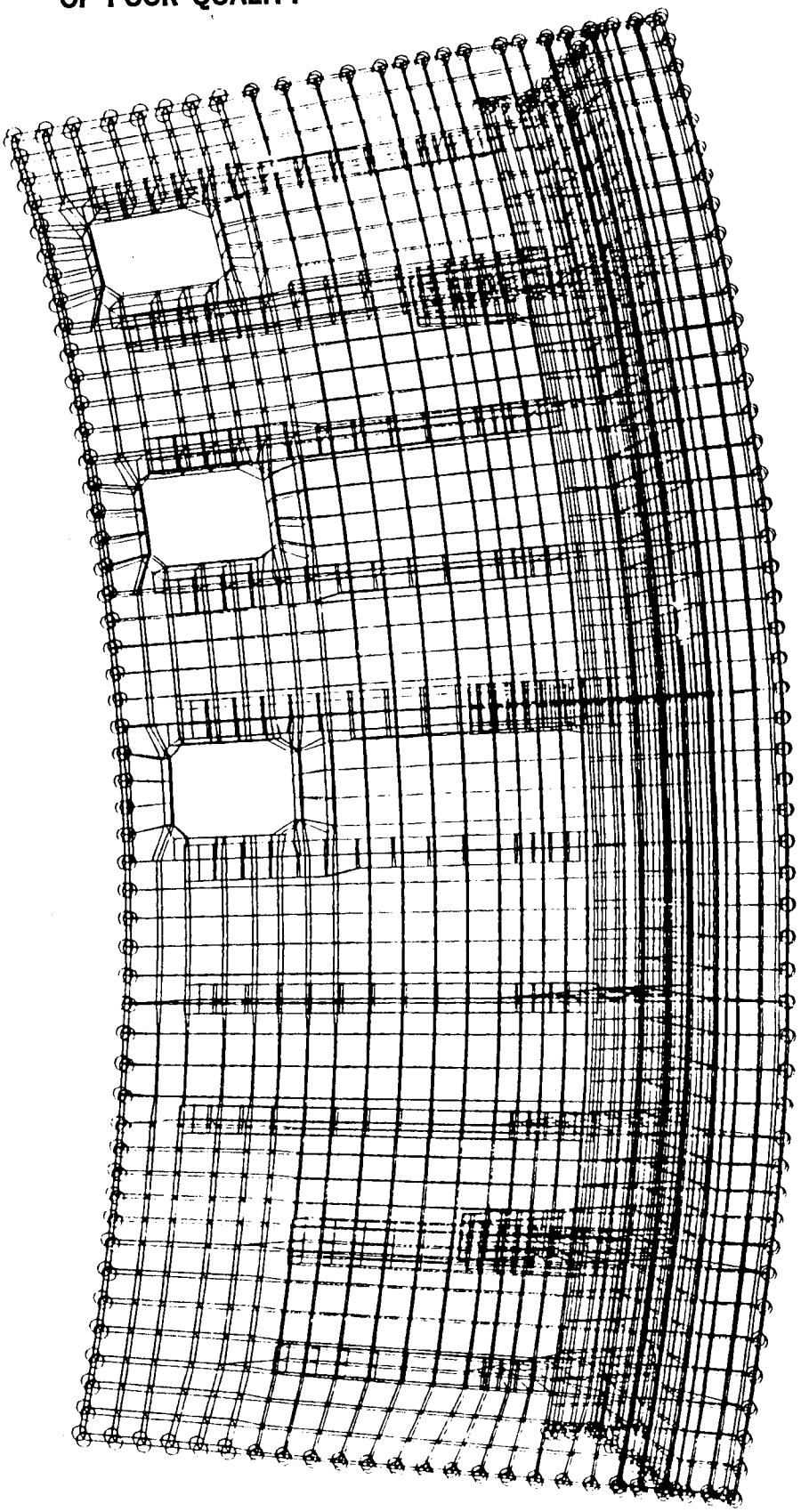

Fig. A-19 Substructure 3B - MRG3
(Substructure Boundary Nodes Circled)

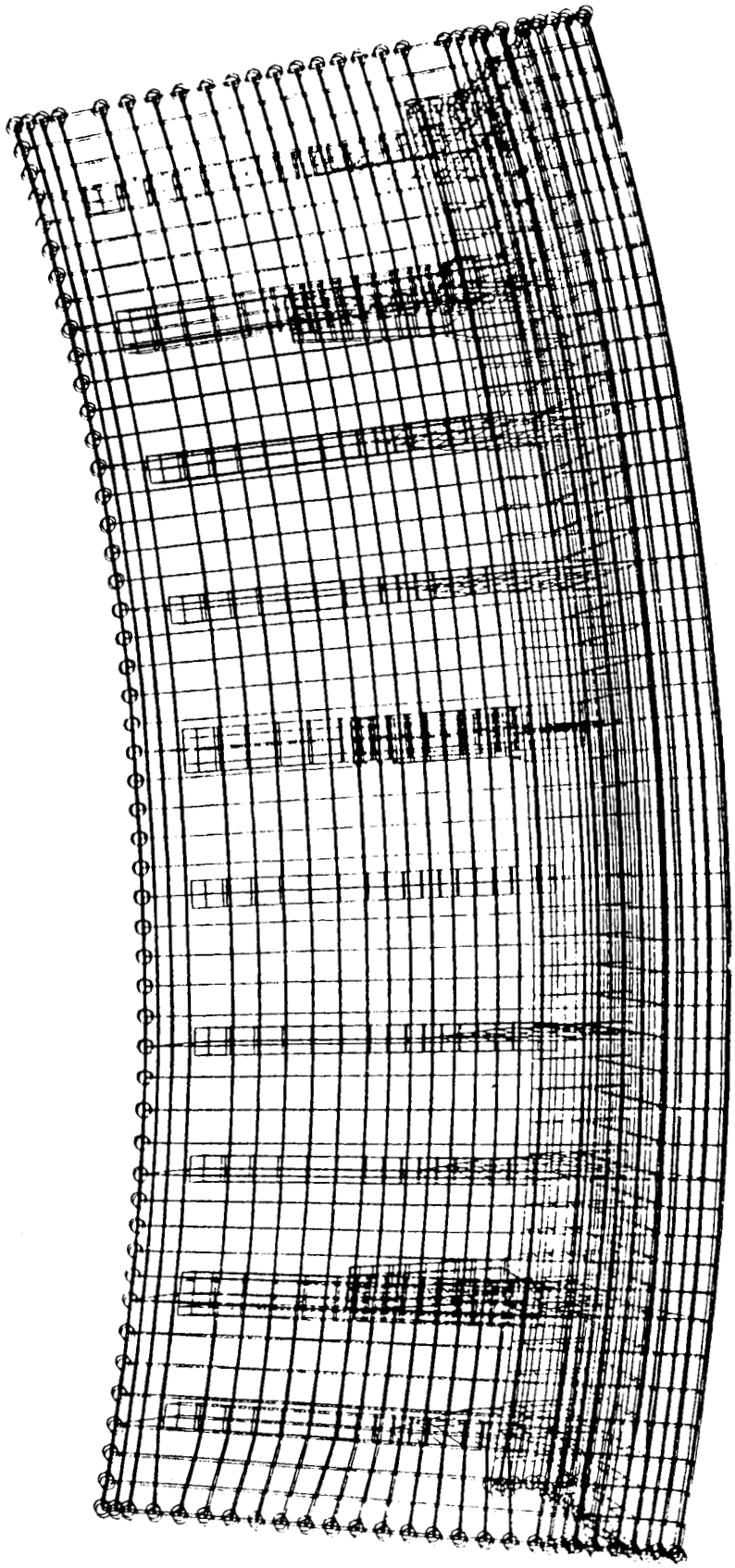

Fig. A-20 Substructure 3C - LRG3
(Substructure Boundary Nodes Circled)